AN ABSTRACT OF THE THESIS OF

Balaji P. Ramamoorthy for the degree of Master of Science in Electrical and Computer Engineering presented on January 3, 1997.

Title: Characterization and Comparison of 830 nm Laser Diodes Fabricated in MOCVD and MBE Grown Heterostructures.

Abstract approved: _____

Thomas K. Plant

This thesis reports on the fabrication and characterization of index-guided, 830 nm laser diodes. These devices were fabricated on MOCVD and MBE grown graded-index separate confinement heterostructures. Material, electrical and optical characterization at room temperature were performed on laser diodes of widths 10 μm, 8 μm, 6 μm and 4 μm, on the two different materials. The main goal of this thesis is to compare these devices fabricated on different materials and investigate their suitability for use in fabricating traveling-wave amplifiers (TWAs). The TWAs made from these devices would be used for study of quantum fluctuations and on effects of gain saturation and amplitude-to-phase coupling on the optical spectrum.

Room temperature photoluminescence experiments are done using 633 nm and 488 nm excitation. Also a novel technique for determining the carrier concentration in the

active region of anisotype heterostructures is presented. Threshold current densities determined from the L-I plots for lasers both the materials were comparable. The output power of the MOCVD lasers was found to be almost double the MBE lasers for similar structures and lengths. Spectral gain results reveal that the MOCVD lasers lased in the 830 ± 20 nm range as specified by the manufacturer. The MBE lasers lased at 8165 Å indicating that the quantum well might be narrower than originally designed. Both the MOCVD and MBE materials are found to be promising for the fabrication of laser diodes and TWAs.

Characterization and Comparison of 830 nm Laser Diodes Fabricated in MOCVD and MBE Grown Heterostructures

by

Balaji P. Ramamoorthy

A THESIS

Submitted to

Oregon State University

in partial fulfillment of

the requirements for the

degree of

Master of Science

Completed **January 3, 1997**

Commencement **June 1997**

Master of Science thesis of Balaji P. Ramamoorthy presented on January 3, 1997

APPROVED:

Major Professor, representing Electrical and Computer Engineering

Head of Department of Electrical and Computer Engineering

Redacted for privacy

Dean of Graduate School

I understand that my thesis will become part of the permanent collection of Oregon State University libraries. My signature below authorizes release of my thesis to any reader upon request.

Redacted for privacy

Balaji P. Ramamoorthy, Author

ACKNOWLEDGMENTS

I would like to extend my gratitude to Dr. T. K. Plant for his moral and financial support, advice and patience which played an important role in the completion of this thesis. I am also grateful to Dr. S. Subramanian for the various tips that he provided during device processing and characterization that kept the project on the move despite various difficulties. I would like to thank Dr. S.L.Lu for his encouragement and taking time to serve on my committee.

I would also like to thank Leon Ungier for his time and effort in doing the MBE crystal growth for the laser material and also general assistance in the clean room. Special thanks to Darren Ferwalt for his assistance in wire bonding.

Financial support provided to this project by NSF grant number ECS-9212997 is gratefully acknowledged.

Last, but not least, I would like to express my thanks and sincere appreciation to my mom, dad, brothers and sister-in-law for their emotional support which meant so much in the realization of this goal.

TABLE OF CONTENTS

TABLE OF CONTENTS (CONTINUED)

LIST OF FIGURES

LIST OF FIGURES (CONTINUED)

LIST OF FIGURES (CONTINUED)

Characterization and Comparison of 830 nm Laser Diodes Fabricated in MOCVD and MBE Grown Heterostructures

1. Introduction

Modern communication systems and fiber optic networks demand light sources with high output power and quantum efficiency with minimal loss of light energy during transmission. Semiconductor lasers play an important role in providing a highly reliable and directed coherent source of light in such communication applications. They are also used in laser printers, compact disk players, medicine, aerospace technology and numerous other scientific applications. Semiconductor lasers have evolved over a period of time with improvements in material growth, device fabrication and characterization techniques. Advances in epitaxial growth of heterojunctions and quantum wells have added new dimensions to the device characteristics and applications of laser diodes.

The most prevalent materials used for laser fabrication are the GaAs/AlGaAs and InGaAs/InP binary-ternary compound systems. The GaAs/AlGaAs system has minimum defects due to the close match of lattice constants between AlAs(5.965 Å) and GaAs(5.966 Å) which are the two parent binary compounds of this system. GaAs/AlGaAs based laser diodes have been made to lase from the red to the near infra-red region of the spectrum, typically from 680 nm to 850 nm.

This thesis reports on the fabrication and characterization of laser diodes (LDs) in MOCVD and MBE grown AlGaAs/GaAs graded index separate confinement heterostructure (GRIN-SCH) materials with a 58 Å wide GaAs quantum well active

region. The objectives of this work are to develop the necessary fabrication processes to successfully fabricate, mount and then to compare the electrical and optical characteristics of 830 nm LDs made from (1) MOCVD GaAs/AlGaAs GRIN-SCH laser material bought from Epitaxial Products, Inc in Cardiff, Wales and (2) from similar composition MBE material grown in-house at OSU. This laser-quality material is designed to have a peak emission of 830 ± 20 nm. The LDs are primarily to test the material and the fabrication process to fabricate long active region traveling wave amplifiers (TWAs). The TWAs are needed for an NSF grant (in collaboration with Prof. M.G. Raymer at the University of Oregon) to study quantum noise propagation in long, traveling-wave semiconductor amplifiers and superluminescent sources. High gain, low loss traveling wave amplifiers with long active regions are required and are not commercially available. Knowing the effects of gain saturation and amplitude-to-phase coupling on the optical spectrum and intensity fluctuations of these sources is important for developing low noise, broad band, high power sources for fiber gyroscopes, tunable lasers and other applications. The AlGaAs/GaAs system (with emission wavelength at 830 nm) was chosen as the material for fabrication of the LDs in this project in order to use an available Ti:Sapphire laser at 830 nm as the input source to the optical amplifiers. TWAs are simply single pass laser structures with no optical feedback. This is usually accomplished by applying coatings to the ends of the laser to eliminate any reflection at the semiconductor/air interface. TWAs exhibit high optical bandwidth, high saturation power and low polarization sensitivity. On the contrary due to low (hopefully, zero) facet reflectivity, they have lower signal gain and higher spontaneous emission. TWAs are difficult to fabricate due to the high quality

antireflection (AR) coatings required. An alternative method can also be used to make the TWAs. The facets are cleaved so that they are inclined at 5°- 7° to the normal. This method has been reported elsewhere to yield high unidirectional amplifier gain with little facet feedback [Zah et al. 1987].

Chapter 2 briefly describes the working principles of semiconductor lasers in general and GRIN-SCH lasers in particular. The operation of a TWA is explained in detail and a survey of different reported fabrication methods for lasers and TWAs are discussed. In Chapter 3 details of the experimental techniques for characterizing the epitaxial materials used to fabricate the laser diodes are presented. Results from photoluminescence experiments and capacitance-voltage measurements are discussed and summarized. The laser fabrication process including masking, photolithography, developing, dry etching, silicon dioxide deposition, metalization, electroless gold plating, lapping, cleaving, bonding and packaging, is discussed in chapter 4 as are the variations needed for making the TWAs. Electrical and optical characterization results such as I-V, L-I and spectral gain characteristics are also presented in chapter 5. Finally the results of material and device characterizations have been summarized and further future work is discussed in the last chapter.

2. Background

2.1 Principles of semiconductor laser operation

The operation of semiconductor lasers is based upon Einstein's relations for stimulated absorption, spontaneous emission and stimulated emission. Lasing refers to stimulated emission that occurs under the conditions of population inversion. Population inversion is a condition in which the system is pumped so that the valence band contains many free holes and the conduction band contains many free electrons at the same position in the material (the active region). Under this condition a photon is more likely to cause the downward transition of an electron from the conduction band to the valance band with the emission of a photon than the upward transition from the valance to the conduction band with the absorption of a photon and stimulated emission occurs instead of absorption. Bernard & Duraffourg [Bernard et al. 1969] showed that the separation of the quasi-Fermi levels must exceed the photon emission energy for the downward stimulated emission rate to exceed the upward absorption rate. This is known as the Bernard and Duraffourg condition for stimulated emission in semiconductors.

The various techniques available to modify the epitaxial layers at the micron and submicron level have made it possible to enhance the efficiency of semiconductor lasers. The efficiency of a laser might drop considerably due to leakage of carriers or light from the active region or due to non-radiative recombination in the active region. The former

occurs due to improper device geometries and refractive index differences between the active region and the adjoining layers. The non-radiative processes can be minimized to by reducing the number of deep levels within the bandgap through improving crystal quality.

The carrier and optical confinement within the active region can be improved by using a double heterojunction structure where interfaces between two dissimilar semiconductor materials surround the active region. The bandgaps of the materials enclosing the active region are larger than that of the active region itself so that the injected carriers are tightly confined to the active region. The larger bandgap cladding materials also have a smaller refractive index than the active region causing the emitted light to be more confined to the active region by optical waveguiding effects. The most widely used heterostructure system for the fabrication of diode lasers (due to the CD player industry) is the GaAs/$Al_xGa_{1-x}As$ system. The emission wavelength of lasers can be varied by varying the Al concentration in the active region and cladding layers, always keeping the cladding layers of larger bandgap. $Al_xGa_{1-x}As$ remains direct bandgap until x=0.4. Epitaxial techniques can be conveniently used to fabricate DH lasers using GaAs/$Al_xGa_{1-x}As$ system in the wavelength range of 680-850 nm. A DH structure under forward bias is shown in Fig(2.1). As shown in the figure the electrons and holes climb the potential barrier to radiatively recombine in the active region. The active region becomes a region of high gain under these conditions. There is also some loss of optical modes in the adjacent cladding layers.

The only distinction between the DH laser and a quantum well laser is the thickness of the active region which is of the order of 0.1 to 0.3 μm in DH lasers and

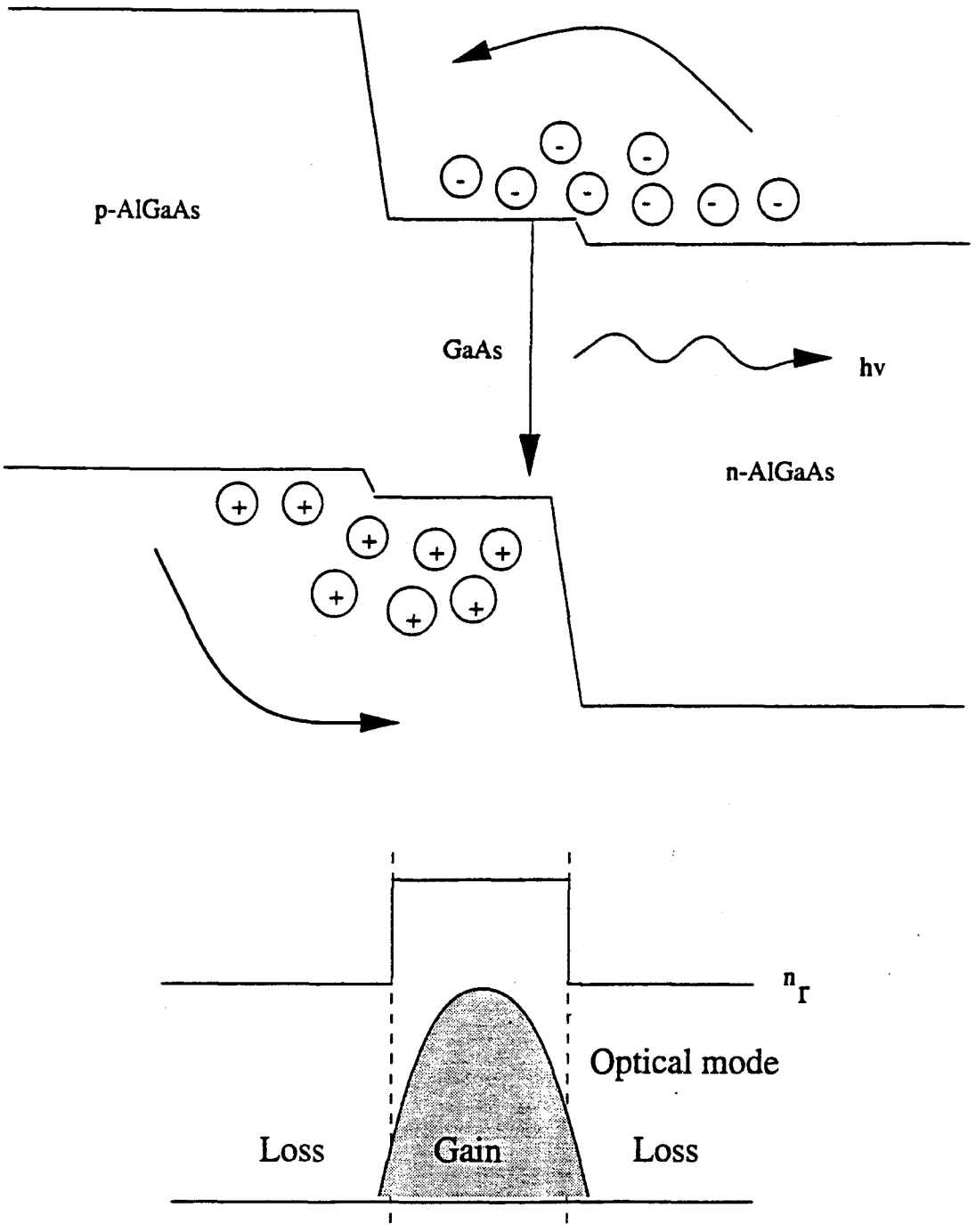

Fig(2.1). A double heterojunction under strong forward bias condition.

about 50 - 100 Å in quantum well lasers. The quantum-size effects change the wavelength and increase gain but they also make the width of the gain region small which causes poor optical confinement. GRIN-SCH lasers overcome the problem of poor optical confinement in quantum well lasers by adding a separate optical confinement region around the active region.

The GRIN-SCH structure is formed of compositionally graded AlGaAs layers that form an optical waveguide which confines the light in the active region. The variation of the index of refraction enhances the optical confinement while the bandgap gradation acts to funnel the injected carriers into the quantum well. The amount of light confined to the active region is measured by a quantity called the optical confinement factor Γ. Γ is a measure of modal confinement and is defined as the fraction of optical intensity in the active region. The optical confinement factor is a strong function of active region thickness and an asymmetry factor η_a defined as:

$$\eta_a = \frac{n_{r2}^2 - n_{r3}^2}{n_{r2}^2 - n_{r1}^2} \tag{2.1}$$

where n_{r2} is the refractive index of the active region and n_{r1} and n_{r3} are the indices of the adjoining layers.

The very small width of active region ultimately leads to high gain and a reduction in the threshold current density of the GRIN-lasers to less than 50 A/cm^2 [Derry] as compared to the DH lasers where it is of the order of 1000 A/cm^2 [Casey et. al]. The lasers fabricated in this thesis have threshold current densities of 1.9 kA/cm^2. Fig(2.2a) shows the GRIN-SCH structure of the MOCVD grown laser material

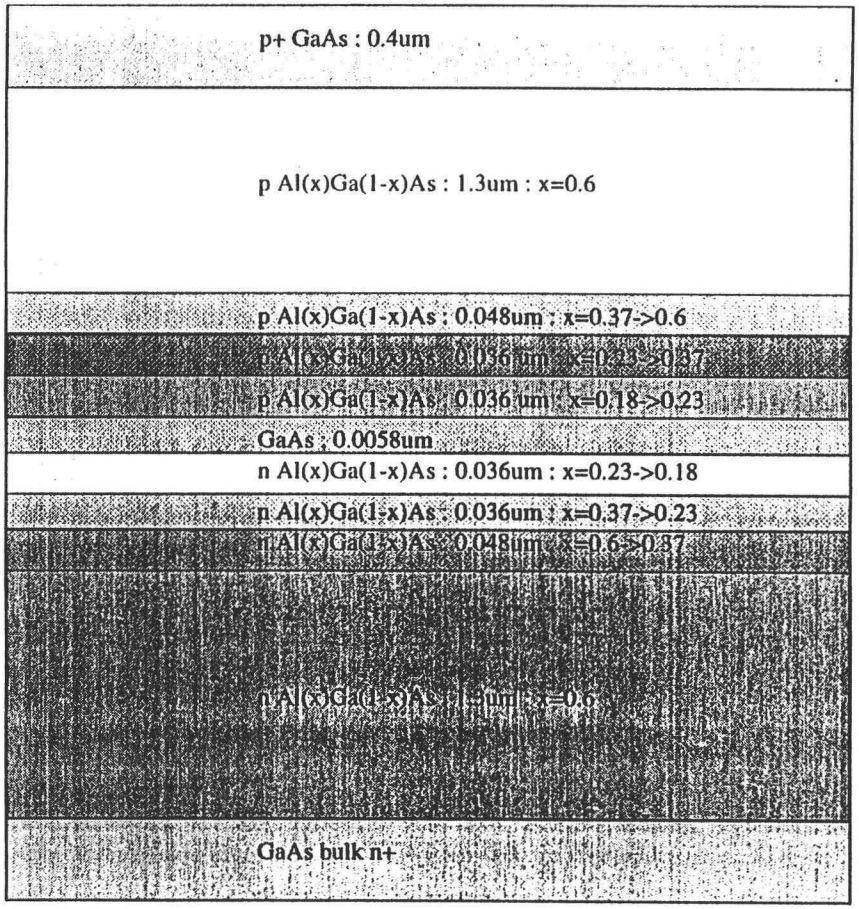

Fig(2.2a) Structure showing different designed layers of the MBE and MOCVD material

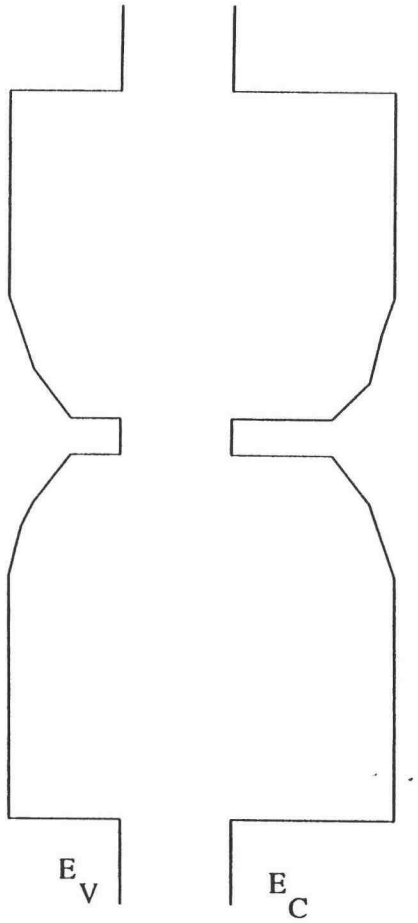

Fig(2.2b) Energy band representation of the structure shown in Fig(2.2a).

used for this thesis. A band representation for this structure is also shown in Fig(2.2b). This structure has an active region of undoped GaAs, 58 Å wide and enclosed by a p- and n-type Al(x)Ga(1-x)As. An active region of this width would yield very low threshold current densities. A graded index region is added in the p- and n-type $Al_{(x)}Ga_{(1-x)}As$ layers grown immediately above and below the active region to a width of 120 nm. The value of x in $Al_{(x)}Ga_{(1-x)}As$ varies from 0.18 next to the GaAs active region to 0.6 next to the outer cladding layers, and this causes a gradual decrease in the refractive index of the layers away from the active region. These layers are in turn sandwiched by a p-$Al_{0.6}Ga_{0.4}As$ cladding on the top and an n-$Al_{0.6}Ga_{0.4}As$ cladding layer on the bottom. A p+ GaAs cap layer and n+ GaAs buffer layer enclose the cladding layers. The bottom buffer layer is to isolate the substrate and form a smooth growth layer. The top cap layer is to improve ohmic contact and isolate the high aluminum content AlGaAs material from oxygen in the air. Details of the composition and carrier concentration are listed in Fig(2.2c). SEM photographs showing a cross section of the MBE material as well as the MOCVD material reveal the various layers. The active region together with the GRIN-SCH layer appear as a very narrow band along the mid-region of the photograph. The different layers appear as different shades of gray due to variation in their optical properties.

A band diagram for this type of structure is shown in Fig(2.3). In this case where there is no external bias, the potential barrier height is too large for the electrons from the adjoining n-AlGaAs and holes from the p-AlGaAs regions to overcome. This results in the active region being devoid of charge carriers required for radiative recombination. In order to facilitate accumulation of charge carriers in the active region and subsequent radiative recombination, a forward bias voltage is applied resulting in a lowering of the barrier

Layer	Material	Mole Fraction (x)	Thickness (μm)	Majority carrier conc. (cm^{-3})	Type	Dopant
11	GaAs		0.4	1E+19	p+	Zn
10	Al(x)GaAs	0.6	1.3	1E+18	p	Zn
9	Al(x)GaAs	0.37 - 0.6	0.048	3E+17	p	Zn
8	Al(x)GaAs	0.23 - 0.37	0.036	3E+17	p	Zn
7	Al(x)GaAs	0.18 - 0.23	0.036	3E+17	p	Zn
6	GaAs		0.0058	Undoped		
5	Al(x)GaAs	0.23 - 0.18	0.036	3E+17	n	Si
4	Al(x)GaAs	0.37 - 0.23	0.036	3E+17	n	Si
3	Al(x)GaAs	0.6 - 0.37	0.048	3E+17	n	Si
2	Al(x)GaAs	0.6	1.3	1E+18	n	Si
1	GaAs		0.5	1E+18	n+	Si

Fig(2.2c). Material specification for the GaAs/AlGaAs MOCVD GRIN-SCH laser structure

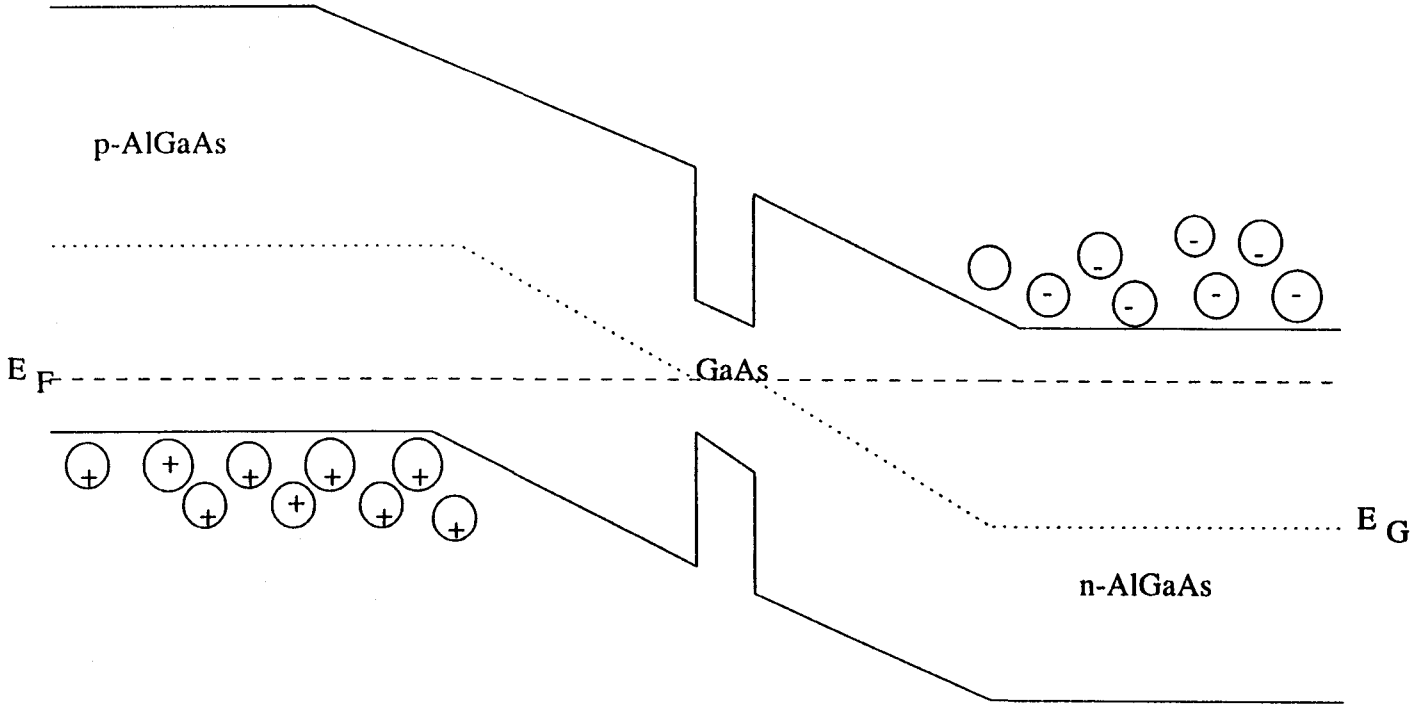

Fig(2.3) Unbiased quantum well laser energy band diagram

climb the barrier and fill the band states in the active region. Energy bands under forward bias condition will be discussed further in chapter 4.

2.2 Working of TWAs

Semiconductor laser amplifiers (SCLAs) have the potential of performing amplification of ultrahigh bandwidth optical signals without having to enter the electrical domain. The SCLAs can be classified into Fabry-Perot (FP) amplifiers and traveling wave amplifiers (TWAs). The FPA is essentially a laser cavity operated below threshold whereas the TWA is an idealized zero feedback device due to antireflection coated facets . The noise filtering characteristics of the FPAs are better than TWAs due to cavity resonances [Thylen]. But the FPAs have very narrow signal bandwidth and also give rise to amplified reflections which, from a systems perspective, could be impractical. For these reasons a TWA (with a reflectance much lower than the 30 percent natural reflectivity of the mirror facets; ideally zero) is generally preferred with provisions for some additional noise filtering. The TWA has superior performance in terms of saturation output, bandwidth etc. It is, however, difficult to rigidly distinguish between FPAs and TWAs since the antireflection coating techniques may not provide complete zero reflectivity. In general, devices with reflectivities less than 0.1 - 1% are regarded as TWAs.

The unsaturated gain spectrum of an InGaAsP/InP 1.5 μm TWA is shown in Fig(2.4) [Shimada et al. 1994]. The TWA has a very broad gain bandwidth. Also the gain peak wavelength shifts to shorter wavelength as the injection current increases. This is due

to band filling effects as shown in Fig(2.5). At high carrier injection levels, the energy difference between the conduction band maximum and valance band maximum in stimulated emission becomes larger. In other words in the high injection state, the peak wavelength shifts to shorter wavelengths as the injection current increases. Due this effect it is essential to start with a laser oscillating at a wavelength longer than the intended high-gain amplification wavelength.

The rate equation can be used to describe the amplification characteristics. The carrier rate equation is given by [Shimada et al. 1994]:

$$\frac{dn}{dt} = -\frac{n}{\tau_s} - \frac{(n-n_O)}{A_g}\frac{I}{hv} + \frac{J}{ed} \tag{2.2}$$

while the propagation of the light signal is given by:

$$\frac{dI}{dz} = \frac{\Gamma\ (n-n_O)I}{A_g} - \alpha I \tag{2.3}$$

where n = carrier density; n_o = carrier density producing gain in the medium; τ_s = carrier relaxation time; A_g = differential gain coefficient (cm^{-2}); I = intensity of light (W/cm^2); J = injection current density (A/cm^2); e = electronic charge; d = thickness of the active layer; h = Planck's constant; ν = frequency of light; Γ = optical confinement factor; α = distributed loss coefficient (cm^{-1}) and z = direction of propagation SCH of light. In the right hand side of Equation (2.2) the first term represents the relaxation process, the second represents stimulated emission, and the third, pumping by current injection. A steady state solution obtained by solving (2.2) and (2.3) is given by:

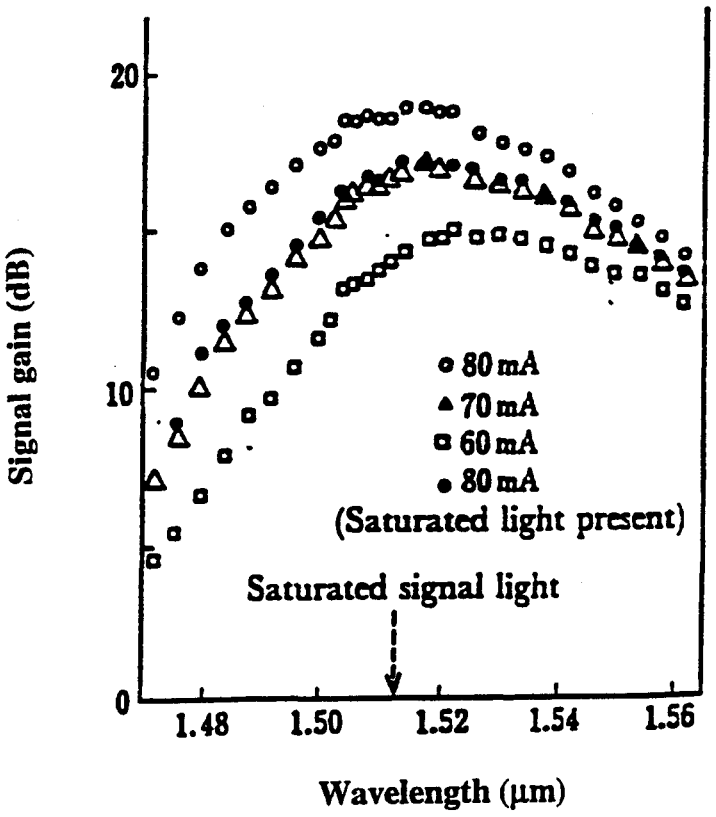

Fig(2.4) Gain spectra [Shimada & Ishio, p46]

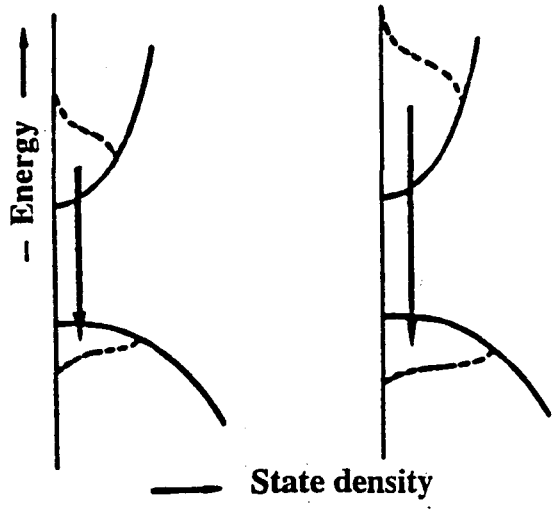

Fig(2.5) Band filling [Shimada & Ishio, p47]

$$\frac{dI}{dz} = \Gamma \frac{\tau_S J / ed - n_O}{A_g (1 + I / I_S)} I - \alpha I = \left(\frac{\Gamma \gamma_o}{1 + I / I_S} - \alpha \right) I \qquad (2.4)$$

where $I_S = \frac{h\nu}{\tau_S A_g}$ represents the saturation intensity and $\gamma_o = A_g ((\tau_s J / ed) - n_o)$ is the unsaturated gain coefficient.

Unsaturated signal gain in a TWA is found by neglecting I / I_s in the denominator of (2.3) and integrating the equation over the amplifier length. We obtain,

$$P_{out} = P_{in} \exp[(\Gamma \gamma_o - \alpha) L] \qquad (2.5)$$

Here, L = the amplifier length, P_{out} = output signal power and P_{in} = input signal power. The exponential term $\exp[(\Gamma\gamma_o - \alpha)L]$ is the signal gain in a TWA. A plot showing the amplifier output power P_{out} as a function of input power P_{in} is shown in Fig(2.6). The light power P and light intensity I are related by $P = S_e I$ where S_e is the light mode cross-section. The equation (2.5) is for an ideal TWA. In actuality the residual facet reflectivity cannot be ignored and hence the resonance effects due to this residual reflectivity must be taken into account. The signal gain G including resonance effects is similar to that of a Fabry-Perot resonator and is given by [Shimada et al. 1994],

$$G = \frac{(1 - R_1)(1 - R_2) G_S}{(1 - \sqrt{R_1 R_2} G_S)^2 + 4\sqrt{R_1 R_2} G_S \sin^2 [2\pi(\nu - \nu_o) L / c]} \qquad (2.6)$$

where R_1 and R_2 are the input and output facet reflectivities, ν is the signal light frequency, ν_o, the resonance frequency of the amplifier and c the speed of light in the medium. As mentioned before, the single pass gain of the amplifier $G_S = \exp[(\Gamma\gamma_o - \alpha)L]$.

Gain saturation in a TWA occurs as the amplification gain decreases with increase in input light power. A theoretical solution for the saturation characteristics of an ideal TWA is found by integrating (2.3) over the amplifier length and is given by [Shimada et al. 1994],

$$I_{out} \exp\left(\frac{I_{out}}{I_s} - \frac{I_{in}}{I_s}\right) = I_{in} \exp(\Gamma \gamma_o L) \tag{2.7}$$

where I_{in} and I_{out} are, respectively, the input and output signal intensities. For a given I_{in}, the I_{out} can be found out by (2.5) and then the gain under saturation can be derived as G = I_{out} / I_{in} .

There are several ways of reducing the reflectivity of the facets in a TWA which have been illustrated in Fig(2.7). The simplest method of reducing reflectivity is to deposit an antireflection coating on the facets of the laser shown in Fig(2.7a). Given a plane wave of wavelength λ incident on a material of refractive index n_s, the refractive index n_f and thickness d_f of the (perfect) antireflection film are given by:

$$n_f = \sqrt{n_s} \tag{2.8}$$

$$d_f = \frac{\lambda}{4n_f} \tag{2.9}$$

It is possible to minimize the reflectivity (practically to zero) by choosing an appropriate value for the refractive index and thickness of the film. Reflectivity below 0.1% has been reported [Saitoh et al 1986] by using SiO for the AR coating. A second method of minimizing reflection effects is by shifting the angle formed by the stripe waveguide

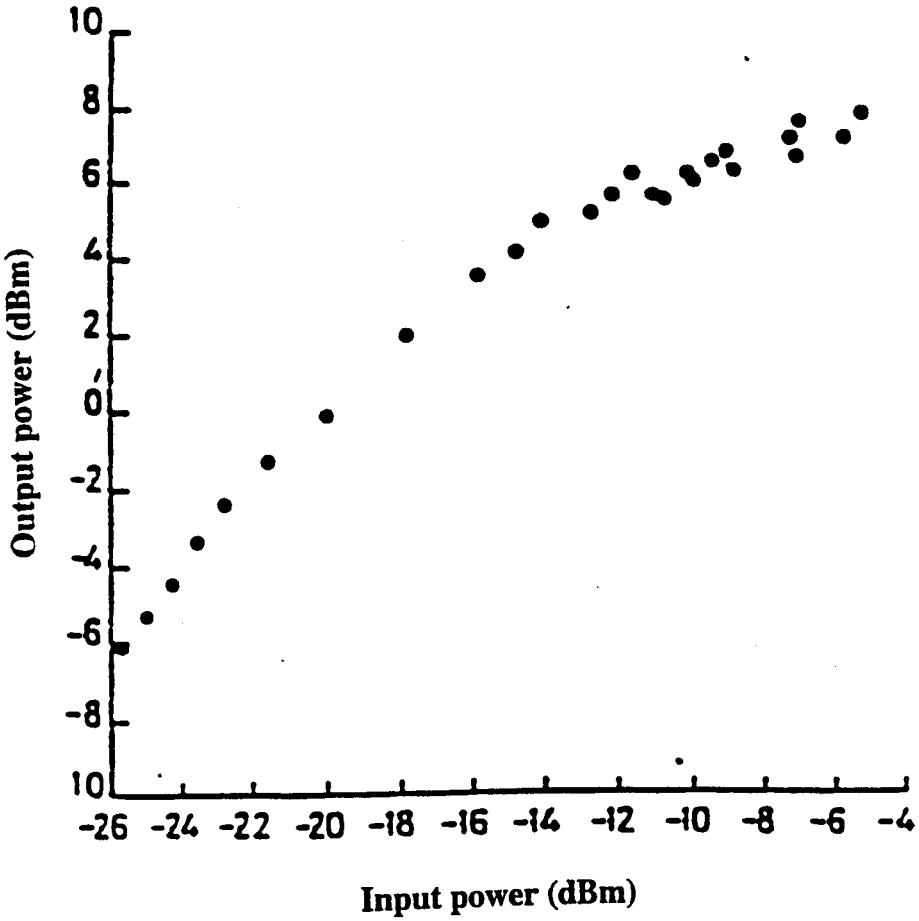

Fig(2.6) Amplifier output power P_{out}, measured experimentally, as a function of the input power P_{in}. [Moreno et al. 1993].

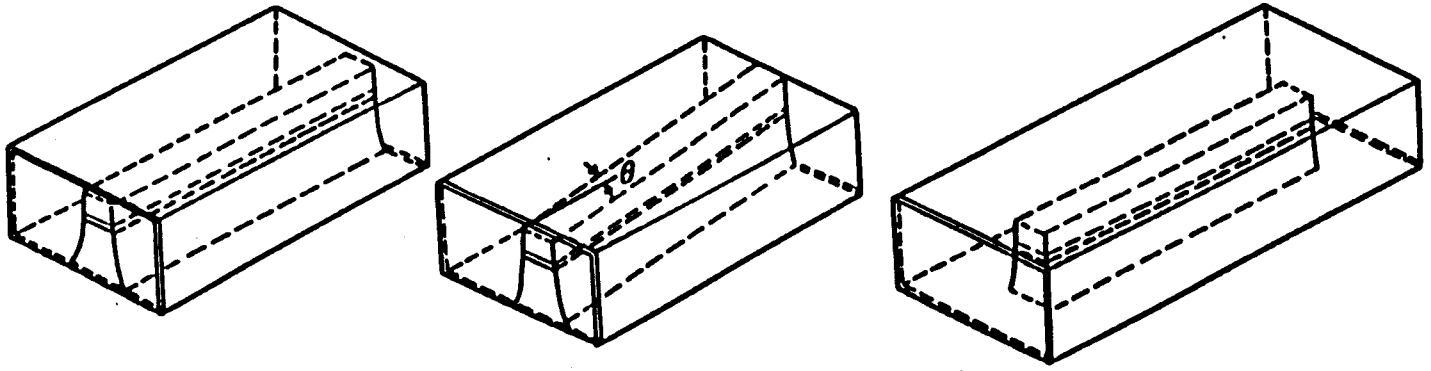

(a) Antireflection coating **(b) Angled waveguide structure** **(c) Window structure**

Fig(2.7) Methods for reducing facet reflectivity [Shimada & Ishio, p74]

containing the active layer and the facets of the TWA away from 90° as shown in Fig(2.7b). Facet reflectivity of 0.2% has been achieved [Zah et al 1987] for an inclination of 7° with the normal. Yet another way of reducing reflectivity effects of the facets is by using a window structure. In this technique, shown in Fig(2.7c), a material with a greater bandgap energy than the active layer is formed near the reflecting surface, so that it becomes a transparent region which will not absorb light and is known as a window region.

2.3 Previous work on TWAs

There have been many publications on semiconductor optical amplifiers. In particular the traveling wave amplifiers have been an area of significant interest. Several people have modeled the gain characteristics [Thylen 1988] [Adams1985] and nonlinear behavior [Moreno et al 1993] of the TWA. These papers report the influence of spontaneous emission coefficient, input power, facet reflectivities etc. on amplifier gain characteristics. Large area AlGaAs/GaAs TWAs [Goldberg et al 1993] [Dente 1993] have been reported to generate high output power up to 21 W.

Present day fiber optic communication systems demand a very high bandwidth at moderate power levels. For this reason most of the TWAs reported in the literature are in the 1.3 μm - 1.55 μm range. The gain characteristics of a 1.3 μm InGaAsP TWA [Wang 1987] are influenced by phenomena like Auger and bimolecular recombination. Fabrication techniques and operating characteristics of the 1.5 μm InGaAsP [Zah et al 1987] [Saitoh

et al 1986] [Mukai et al 1983] TWA have suggested a few methods viz. AR coating techniques and angled waveguides for the reduction of facet reflectivities to obtain reasonable optical bandwidth and signal gain.

3. Material Growth and Characterization

3.1 Introduction

The fabrication of the laser devices involves many steps which are both labor and time intensive. Thus it is prudent to characterize the material to be used for fabrication to be sure it is of high enough luminance to proceed. The key point of interest in the whole GRIN-SCH epitaxial structure is the active region itself and the carrier dynamics within. Another point of interest in the material characterization is the peak emission wavelength around which the devices are expected to emit light.

Heterojunction band offset is an important factor in the design of quantum well lasers. Capacitance-voltage profiling is a useful technique in determining the band offset of a double heterojunction GRIN-SCH structure. This technique has been previously reported for single heterojunctions and for isotype heterojunction systems [Subramanian et. al]. Attempt has been made here to use a similar technique for an anisotype heterojunction system where the active region is sandwiched between two different materials. This technique would help in determining the depth and carrier concentration of the active region.

Photoluminescence (PL) measurements are used to examine the optical quality of both the MBE and MOCVD grown materials. PL measurements give an approximate idea

of the wavelength at which lasers made out of these materials will lase and also some details regarding the quality of active region can be inferred.

A brief outline of the experimental techniques required for these experiments has been given below. Furthermore the results have been presented, analyzed and summarized.

3.2 Experimental methods

3.2.1 PL measurements

The PL setup consists of a laser source to provide photoexcitation, lenses and filters to focus a well-defined excitation beam onto the sample, a monochromator to detect the PL spectra of the emission, a photomultiplier tube(PMT) detector, lock-in amplifier, optical chopper and power supplies. The sample is held in vacuum for low temperature measurements but no vacuum is required for room temperature measurements. The laser beam is focussed onto the sample after passing through the 50% optical chopper and a filter to remove plasma emissions. The light emission from the sample is focussed into the monochromator which is then scanned over a range of wavelengths. The intensities of the corresponding wavelengths being scanned are recorded by the PL software using a data acquisition card to read the lock-in amplifier signal. A plot of wavelength versus intensity is then obtained for the corresponding PL spectra.

The samples used for this purpose were approximately 5 mm X 5 mm square. These samples were etched to a depth of approximately 1.2 μm to remove much of the

AlGaAs cladding layer and allow more of the excitation laser photons to reach the active layer. Initially the etchant used was a solution of $NH_4OH + H_2O_2 + H_2O$ in the ratio 3:1:100. This etchant, calibrated to have an etch rate of 2000 Å/min., caused surface discoloration. Another etchant consisting of $H_3PO_4 + H_2O_2 + H_2O$ in the ratio 3:1:50 and having a calibrated etch rate of 1000 Å/min. was used subsequently, with no surface discoloration.

3.2.2 C-V measurements

Onto the top surface of the material, circular p-ohmic dots of radius 250 μm (approximately) were formed by evaporating the metals as follows: 100 Å Au/350 Å Zn/1000 Å Au. The bottom surface was covered with evaporated n-ohmic metals in the order 100 Å Ni/1000 Å AuGe. The samples are subsequently annealed at 450 °C for 3 minutes. A solution consisting of H_3PO_4, H_2O_2 and H_2O in the ratio 3:4:1 is used to etch the sample about 7 μm deep to form a mesa structure. The etch rate is about 4.5 μm/min. and the sample was etched for about 1 min. and 30 sec. The annealed metal dots are used as the etch mask. C-V measurements are performed at room temperature using an HP4280A capacitance meter at 1MHz. The C-V measurements are performed under reverse bias conditions. A reverse d.c bias is applied, in steps, to the metal dots until the breakdown voltage for the junction is reached. The capacitance value for each voltage step is recorded . The following relations are used to determine the carrier concentration $n(x)$ and the junction depth x [Subramanian et al. 1993],

$$n(x) = \frac{2}{\left(q\varepsilon A^2 \frac{dC^{-2}}{dV} \right)} \tag{3.1}$$

$$x = \frac{\varepsilon\varepsilon_o A}{C} \tag{3.2}$$

where ε is the dielectric constant, A is the area of the diode and q is the electronic charge.

3.3 Results and discussion

3.3.1 PL measurements

PL experiments at room temperature, on these samples yielded very low intensity output and at wavelengths not corresponding to the bandgap of the active region when the 488 nm Ar^+ laser was used as the excitation source. Low temperature (16 Kelvin) measurements were repeated on the same samples and peaks were obtained at 8600 Å with a full width half maximum (FWHM) of 300 Å for the MOCVD material and at 8450 Å with a FWHM of 200 Å for the MBE material. A possible explanation for this behavior could be that the etching is obstructed by an unknown material on the surface produced due to etching with the NH_4OH system, and the laser light used for photoexcitation was mostly absorbed in the surface layers before it could reach the active region. Another etchant consisting of $H_3PO_4 + H_2O_2 + H_2O$ in the ratio 3:1:50 and having a calibrated etch rate of 1000 Å/min. was used for the experiments repeated on fresh pieces of the samples. The samples were etched for 17 min. to obtain a depth of about 1.7 μm. The surface of

the samples did not loose its luster but still the PL output was very weak but larger than for the previous case. A HeNe laser was then used as the excitation source instead of an argon ion laser. The room temperature PL characteristics are shown in the Figs(3.1) and (3.2). These figures show that the MOCVD material has a broad spectrum with a peak intensity at 8400 Å and a FWHM of 250 Å. This is a confirmation of the peak emission wavelength as specified by the manufacturer. The MBE material gave a peak at 8600 Å with a very broad spectrum having a FWHM of 600 Å. The room temperature peak intensities obtained for the PL spectra of the MBE and the MOCVD samples were comparable suggesting that the in-house MBE grown laser sample might also be a good quality material for the fabrication of laser diodes.

Low temperature (19 K) measurements were taken on the MOCVD sample and the peak as expected shifted to a lower wavelength at 8150 A° with a FWHM of 100 Å. When excited with an Ar+ laser similar results were obtained. These results are shown in Figs(3.3) and (3.4). This shift to lower wavelengths is consistent with the fact that at low temperatures the bandgap of the material increases due to contraction of the crystal lattice and strengthening of interatomic bonds. The difference in the peak emission wavelengths for the MOCVD(8400 Å) and the MBE(8600 Å) materials having similar heterostructure design indicates that there is better control of growth parameters in the case of MOCVD growth as compared to MBE growth. Moreover the use of the HeNe laser in place of the Ar^+ laser as the excitation source gave the expected emission spectra. This can be attributed to the very shallow absorption depth for the Ar^+ (488 nm) light which combined with relatively low excitation powers would lead to less number of carriers reaching the

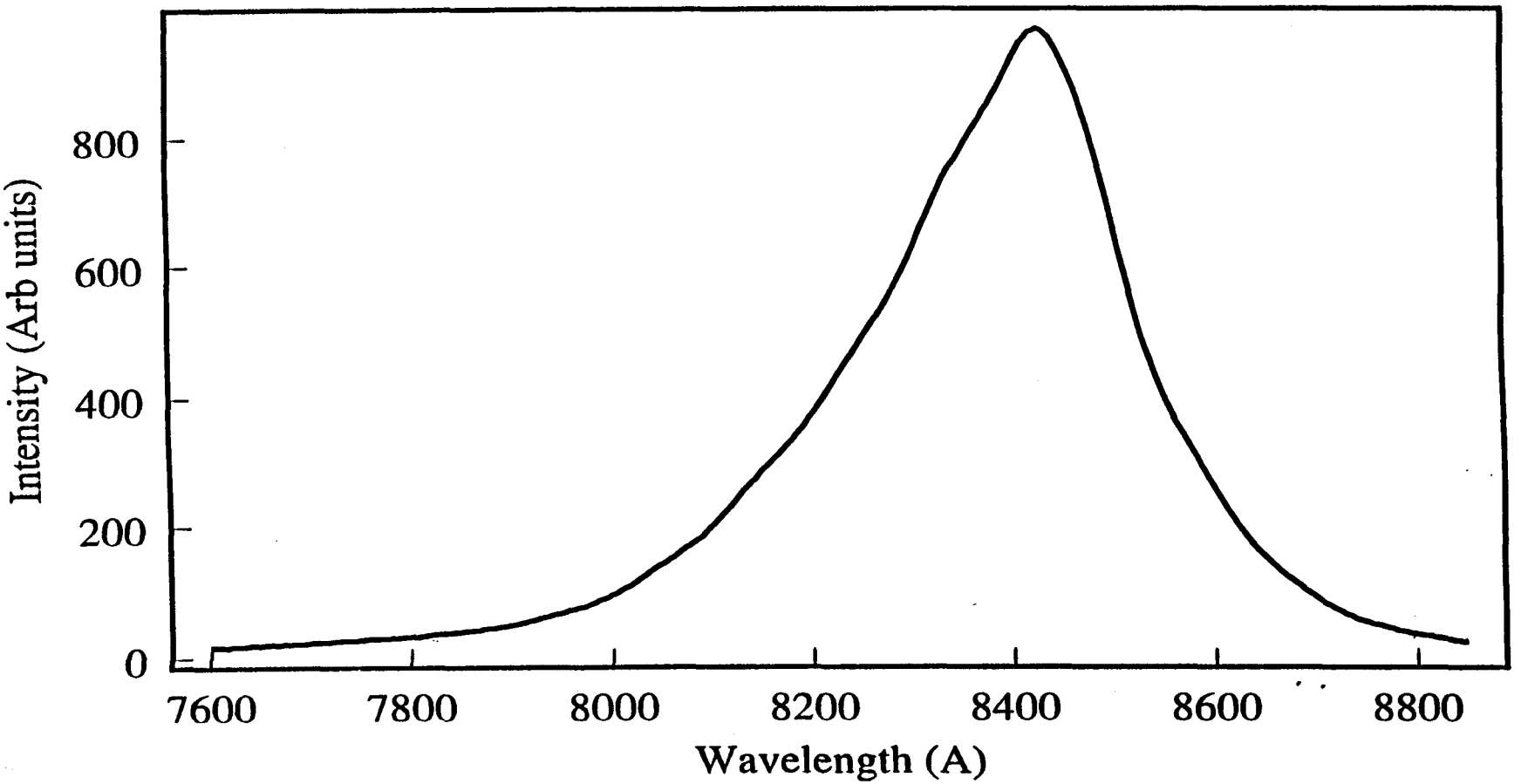

Fig(3.1) PL spectra of MOCVD laser sample @ 300K, excited with HeNe laser source.

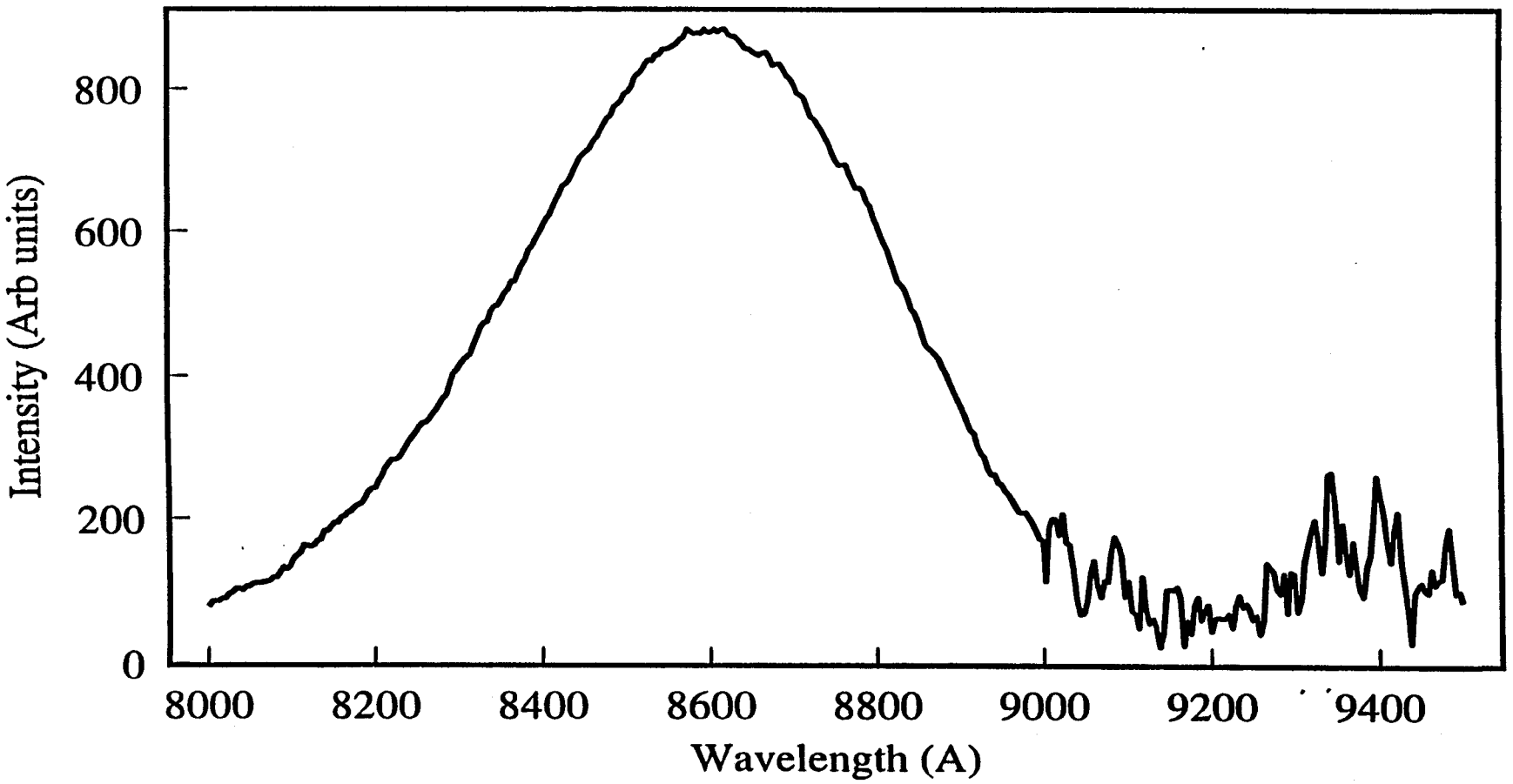

Fig(3.2) PL spectrum of MBE laser material @300K excited with HeNe laser source.

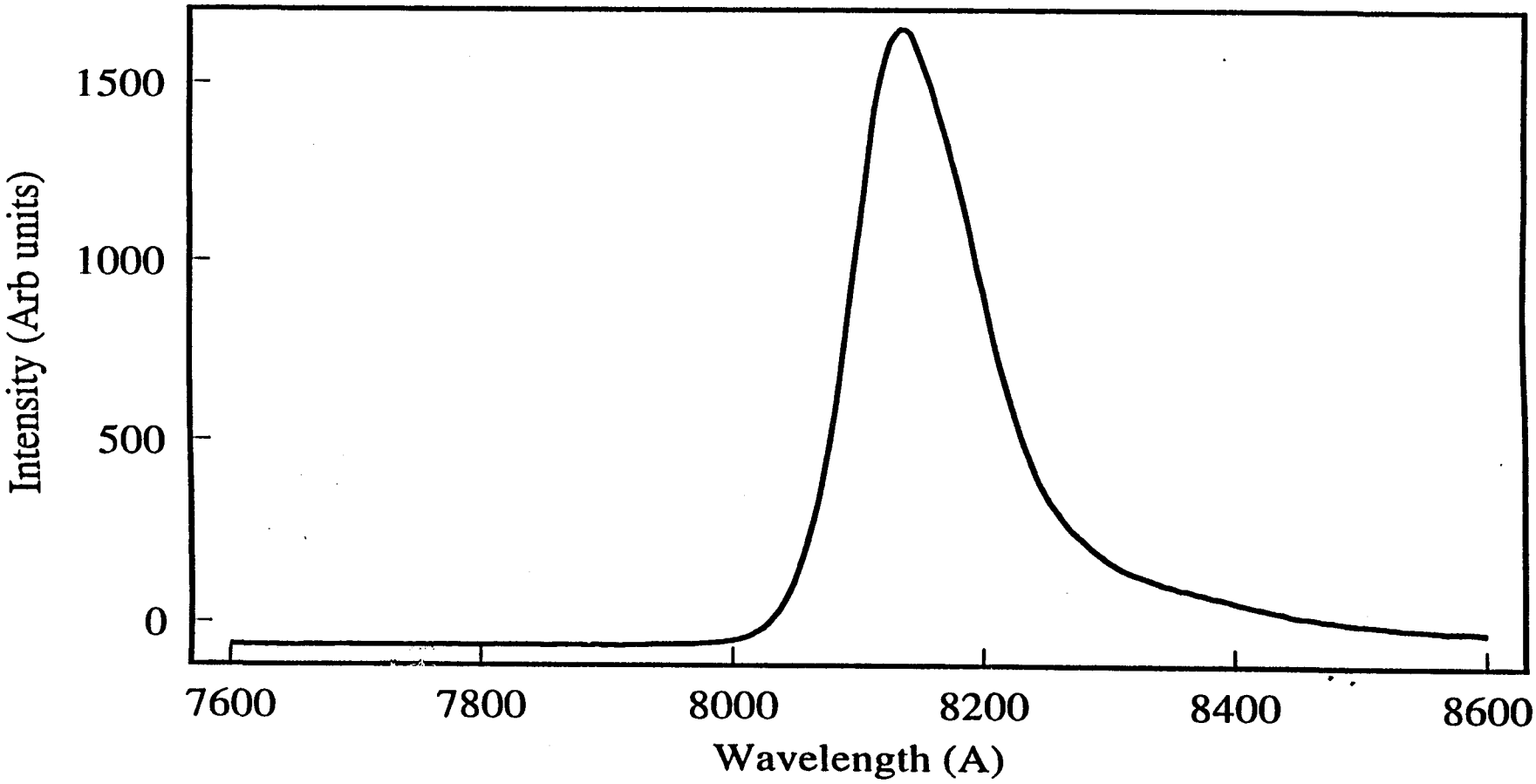

Fig(3.3) PL spectrum of MOCVD material @19K, excited with HeNe laser source

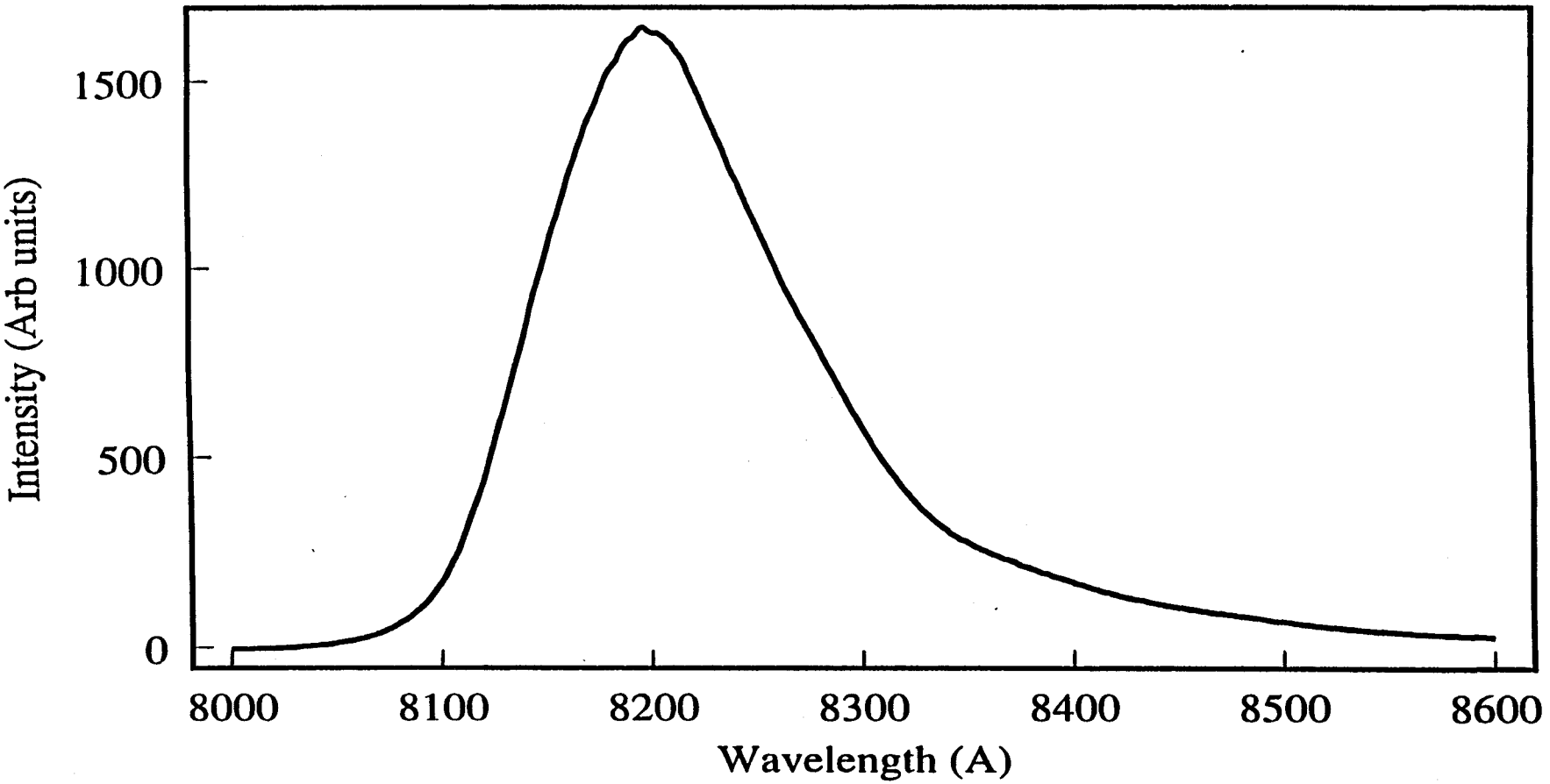

Fig(3.4) PL spectrum of MOCVD material @19K, excited with Ar+ laser source

quantum well and a greater chance of recombination within the barrier regions. Thus at higher temperatures, room temperature for example, the PL signal from the quantum well is likely to become weak due to the sweeping out of the holes by the built in electric field and their conduction away from the highly conductive p-type cladding layer. This 'thresholding effect' for the PL signal can be pronounced for shallow excitation and low excitation powers.

3.3.2 C-V measurements

A reverse bias ranging from 0 V to -6.6 V was applied to the contacts. Capacitance values measured ranged from 251.8 pF for 0 V to 129.8 pF for -6.6 V. The breakdown occurs at about -6.7 V and hence it was not possible to bias the device below -6.6 V. The $1/C^2$ vs V plot obtained is almost linear. This behavior is expected of a normal p-n junction but some deviation is expected for the anisotropic heterojunction system.

The C-V measurements are made to probe the carrier concentration adjoining the quantum well region. The plot of $n(x)$ vs x shown in Fig(3.5) indicates the carrier concentration for the GRIN region extending from about 0.09 μm to 0.18 μm around the quantum well region. The depth of probing could not be increased due to the small breakdown voltages for the laser material. This plot denotes the average carrier concentrations in the p and n regions of the GRIN layer. From the plot it can be deduced that the concentration of the carriers in the 0.09 μm - 0.13 μm region is of the order 3E+17 cm^{-3}. Beyond 0.13 μm up to 0.18 μm the carrier concentration gradually increases

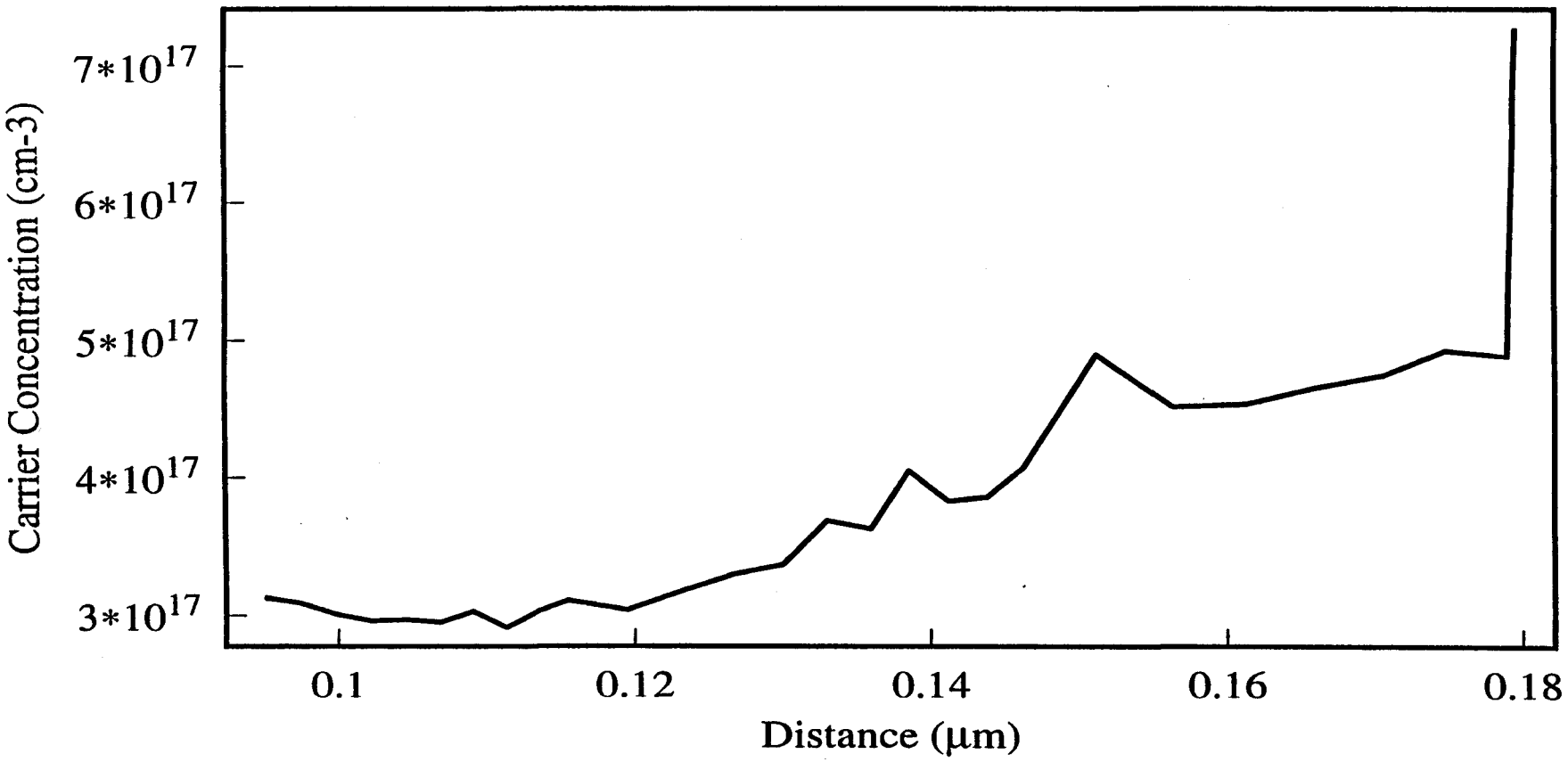

Fig(3.5) C-V measurements on MOCVD grown laser material showing carrier concentration in layers close to the active region.

towards 1E+18 cm^{-3}. These figures are in agreement with the specifications for the carrier concentrations of the different layers grown on the sample. The C-V profile given by the manufacturer of the MOCVD sample was obtained using polaron electrochemical C-V profiling. These profiles verify the carrier concentrations in the p and n cap and cladding layers to be of the order of 1E+19 and 1E+18 cm^{-3}. Thus the C-V measurements performed on these samples is a verification of the carrier concentration in the GRIN layer which was not reported by the manufacturer.

3.4 Summary

To summarize the results from the PL experiments it was found that the room temperature measurements performed on the MBE and MOCVD materials revealed PL signal with peak emission at 8400 Å with FWHM of 250 Å for the MOCVD material and at 8600 Å with a FWHM of 600 Å for the MBE material. The peak emission wavelength of the MOCVD sample confirms the specification provided by the manufacturer. The PL spectra of these materials also indicate the approximate wavelength at which the lasers can be expected to lase.

The C-V data clearly indicates a carrier concentration of 1E+18 in the cladding layer and about 3E+17 in the GRIN layer. This is again a confirmation of the manufacturers specifications for the material. This technique, reported earlier for homojunctions and isotropic heterojunctions, can therefore be used effectively for probing the active regions of anisotropic heterojunctions as in this case.

4. Device Fabrication

4.1 Introduction

The fabrication of the devices involves various processing steps including projection mask lithography, wet and dry etching, thermal evaporation and annealing, silicon dioxide deposition, lapping, electroless plating, cleaving, mounting and wire bonding of the devices. The above mentioned process steps are discussed in the process design section. A new mask for the laser devices was designed using CAD tools for mask design. Details of dimensions of the mask features have been discussed separately in this chapter. TWAs have some specific processing requirements such as AR coating and stripes inclined at a certain angle etc. These issues have also been highlighted later in the chapter.

4.2 Mask design

The mask sets required for this thesis were designed using Mentor Graphics CAD tools for mask design. Only two levels were required for this mask: a first level to define the long stripe regions and the second level for the contact pads. All stripes designed in level one were 12 mm long and of widths of 4 μm, 6 μm, 8 μm and 10 μm. A spacing of 150 μm was kept between the stripes. After every two repetitions of the stripes of

different widths, a spacing of 200 μm was inserted before repeating the next set of stripe patterns. The second level mask contains long stripes of width 20 μm and length 12 mm. Along these stripes contact pads of size 350 μm X 100 μm were placed at intervals of 150 μm. This was done along the entire 12 mm length of each of the 20 μm wide stripes. The mask was designed to fit the two levels into the upper half of a 2 inch square area. The projection mask aligner at OSU is capable of holding a 2.5 inch square mask. Also the dimensions of the pattern on the mask were made twice the actual dimensions of the patterns intended on the wafer since our Canon Model FPA-120 aligner does a 2:1 reduction when transferring the pattern from the mask onto the wafer. The different levels of the mask set designed for this thesis are shown in Fig(4.1) and Fig(4.2). The mask design was subsequently translated on a glass-chrome metal mask fabricated by Photomask Inc..

4.3 Process design

The process steps for fabrication involve the use of two mask levels of required polarities depending upon whether a liftoff process or an etch process is followed. A complete description of the different steps follows:

4.3.1 Level 1: stripe geometry p-ohmic contact

1) Clean the sample with acetone, methanol and deionized water (AMD process) and blow it dry with N_2.

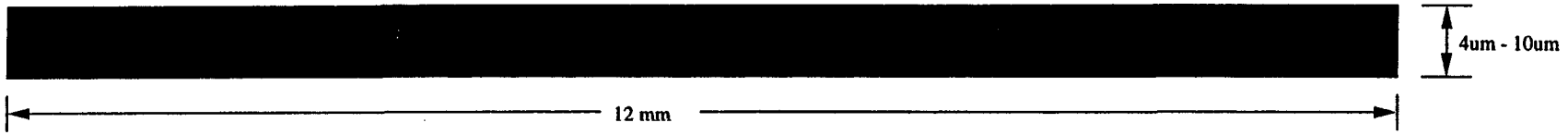

Fig(4.1a) Level 1 mask with dark stripe regions.

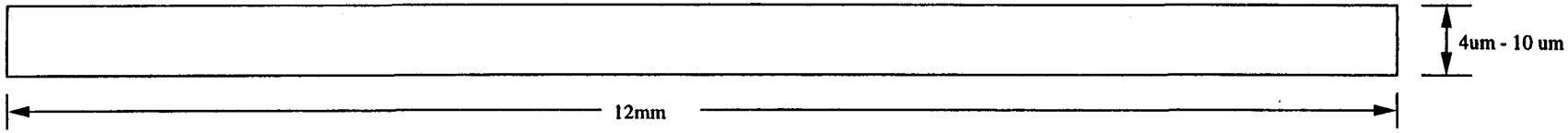

Fig(4.1b). Level 2 mask with transparent regions.

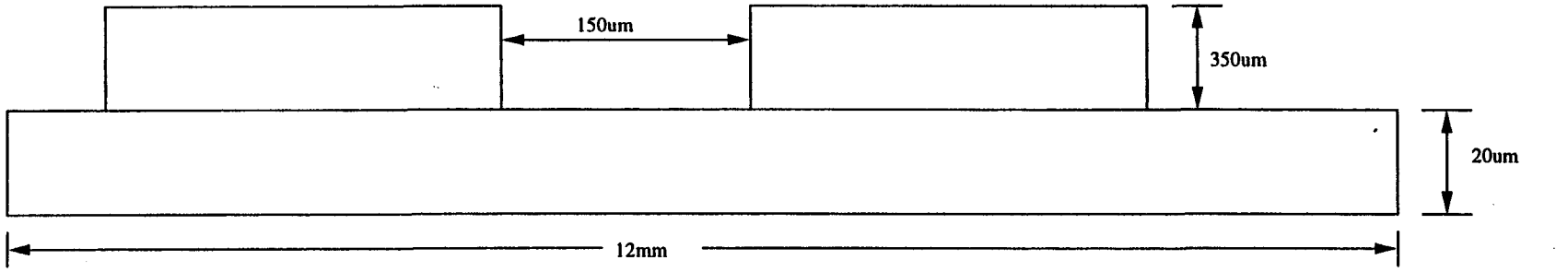

Fig(4.1c) Level 3 mask with transparent bonding pad region.

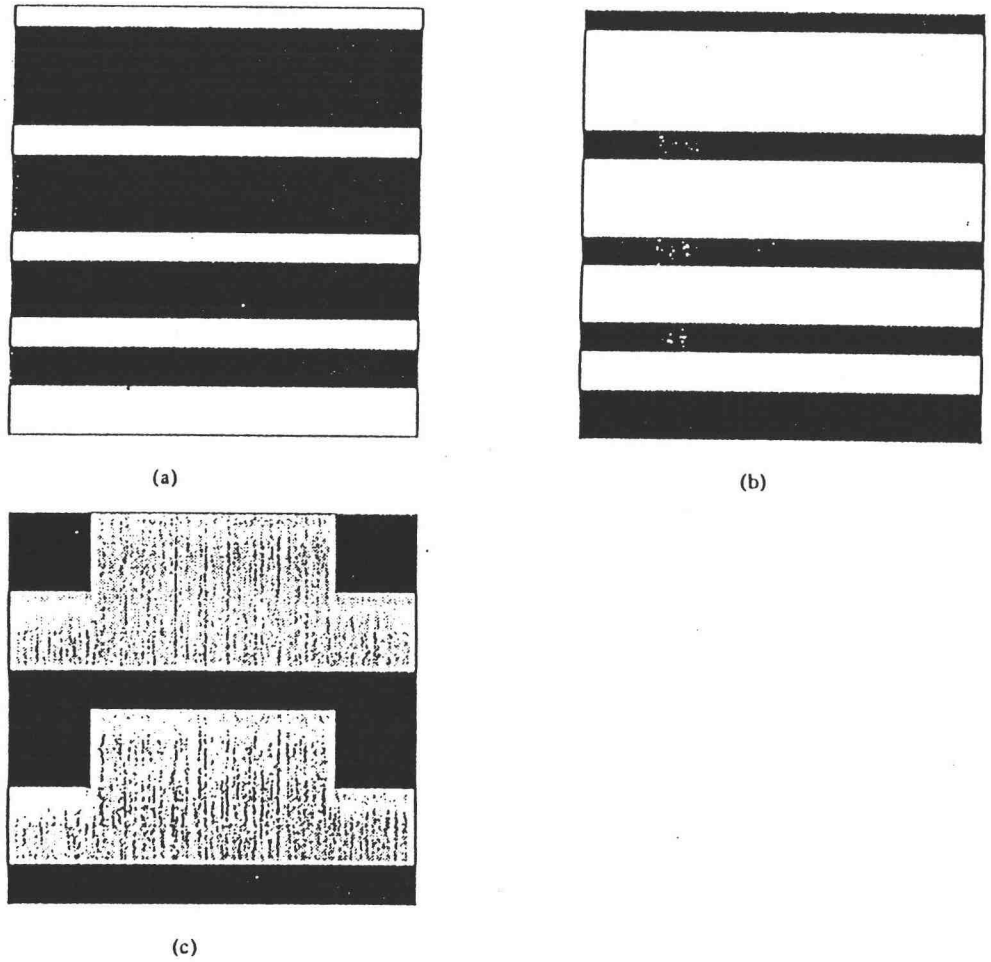

Fig(4.2) (a) Level 1 (b) Level 2 (c) Level 3 masks.

2) Dip sample in $NH_4OH:H_2O$ solution in the ratio 1:3 to remove surface oxides. Wash it with DI water.

3) Load the sample on a holder for thermal evaporation. Evaporation for the p-ohmic metals is done in the sequence 150 Å Ti, 150 Å Au, 350 Å Zn, 1500 Å Au.

4) Spin photoresist (Shipley Corp.) @ 4000 rpm for 40 seconds on the sample coated with p-ohmic metal.

5) Soft bake @ 85 °C for 10 minutes to remove solvents.

6) Using the level 1 mask (Fig (4.2a)) for stripe geometry and with a polarity such that the stripe pattern obtained on the sample remains unexposed, expose the sample through the mask with ultraviolet light.

7) Dip the sample in chlorobenzene for 5 minutes. This helps to harden the uppermost resist layer which in turn results in a protruding top edge (for easier liftoff) profile during development.

8) Develop the sample in developer (Microhard 319, Shipley Corp. used for this process. Developing time was calibrated to 40 seconds).

9) Hard bake the sample after rinsing with DI water for 5 minutes @ 130 °C.

10) Etch the sample in a gold etchant prepared by mixing $KI/I/H_2O$ in the proportion 4 gm/1 gm/40 ml. This etching should be performed only briefly from 5 seconds to not more than 20 seconds. A prolonged etch would

result in the appearance of undesirable hidden features or scratches on the sample.

11) Wash the sample in DI water and perform mesa etch. The mesa etch is done by dipping the sample in a solution of H_3PO_4:H_2O_2:H_2O in the ratio 3:1:50 for 12 minutes. The calibrated etch rate is 1000 Å/minute. Thus a total of about 1.2 μm of etch depth can be obtained.

12) Wash off the photoresist from the sample and anneal the p-ohmic metal stripes. Thermal annealing was used for this purpose. The annealing was done at a temperature of 450 °C for 3 minutes.

4.3.2 SiO_2 deposition by spin on method

Device isolation is done by providing insulation between devices. PECVD SiON is usually used for this purpose, but this was not possible due to problems with the CVD reactor. Therefore SiO_2 was used as an insulator for this process. Silicon dioxide can be deposited on the substrate using a special substance called "spin on glass" supplied by Silica-Source Technology Corp. Tempe, AZ. Non-doped glass in liquid form is applied on the substrate and spun at 3500 rpm for 10 seconds. It is immediately heated in a convection oven at 140°C for 60 minutes. The color of the SiO_2 film interference filter changes from deep violet to somewhat pink or purple indicating a thinning of the film. This film was found to have good adhesion to the sample. If necessary the sample could be

further annealed at 400°C for 60-90 minutes to densify the glass. Non-doped glass is very sensitive to moisture and therefore this procedure is to be performed at humidity levels less than 40%.

4.3.3 Level 2: etching windows in SiO_2

The level 2 lithography step is required to open windows on top of the annealed p-ohmic metal stripes. SiO_2 would subsequently be removed by reactive ion etching. The mask for level 2 is shown in Fig(4.2b). All other steps for lithography and pattern development is the same as outlined in section 4.3.1.

The reactive ion etch was used to etch the SiO_2 from the stripe region. This etching technique provides a very sharp etch profile and does not result in any significant undercutting. This is useful when the feature sizes are very small. The etching is carried out in a vacuum chamber at a low pressure of the order of 10^{-4} torr. The reactant gases used in this case are CHF_3 (Fluoroform) and O_2. These gases, maintained at about 15 psi, are mixed in the chamber and RF power is applied between the electrodes in the chamber to strike a plasma. This procedure was carried out in a BatchTop VII RIE system with complete computer controlled operations. A three minute etch recipe was used for this purpose. Hard baked photoresist acts as an efficient etch mask. A photograph of the device after the completion of this level is shown in Fig(4.3). Perfect alignment of stripes is shown in Fig(4.4).

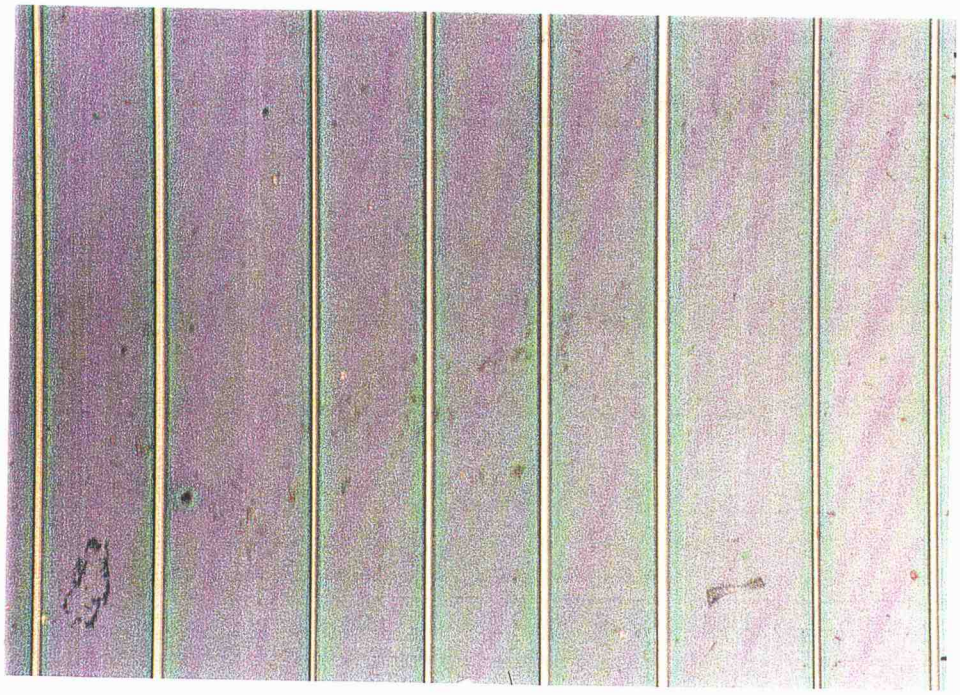

Fig(4.3) Photograph showing the devices after the end of level 2 lithography.

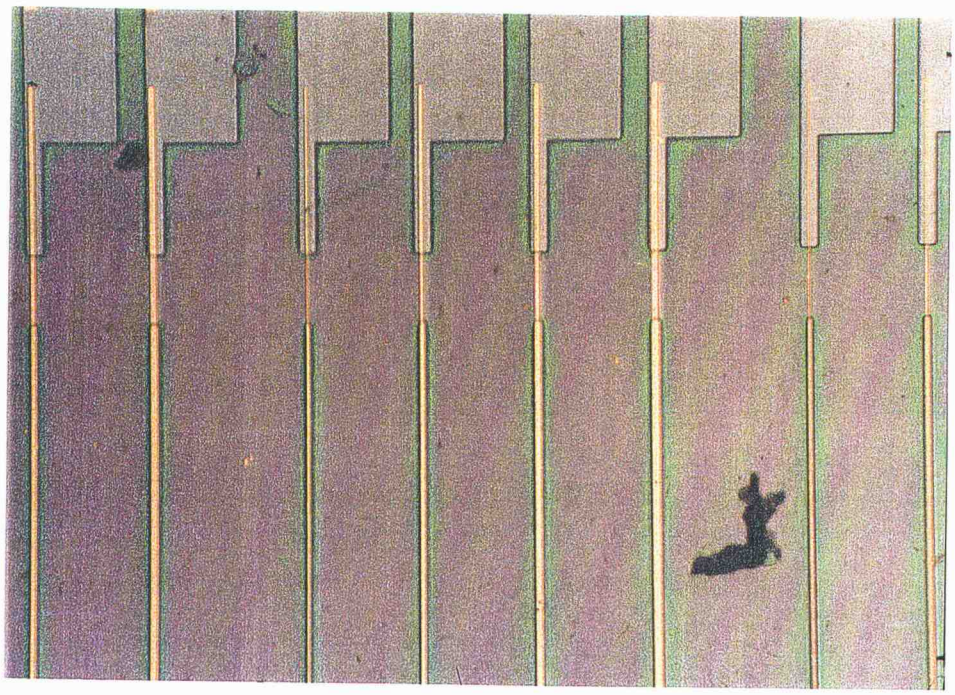

Fig(4.4) Photograph showing perfect alignment of the stripes.

4.3.4 Level 3: contact pad lithography

Contact pad lithography is performed in order to provide a thick metal layer on the stripe regions for good electrical conduction. The various steps required for this process are as follows:

1) Clean the substrate with acetone, methanol and deionized water and dry with N_2.

2) Spin photoresist @ 4000 rpm and soft bake it for 10 minutes @ 85 °C.

3) Align the contact pad patterns on the stripes. The mask used here (Fig (4.2c)) is such that the pad regions are exposed.

4) After a 5 minute chlorobenzene dip develop the sample in a developer.

5) Hard bake the sample @ 130 °C for 5 minutes.

Fig(4.5) shows a photograph of the devices after the completion of this step.

4.3.5 Bonding pad metalization using electroless gold plating

The bonding pad metal ideally should be thick in order to facilitate wire bonding. This is easily achieved by the electroless plating process. The electroless plating based on gold potassium cyanide can only be done on nickel. For this reason Ni is deposited on the sample with the bonding pad pattern on it so that after lift off, Ni remains only in the pad regions. The procedure followed is summarized below:

1) Deposit 250 Å of Ti and 350 Å of Ni by thermal evaporation.

2) Lift off the metal using acetone. Ni will remain only in the bonding pad areas.

3) The sample is then put in the electroless gold solution kept at 90 °C for 10 minutes. This would plate up to 25 KÅ (calibrated) of gold.

4) Rinse the sample thoroughly with deionized water.

Photograph of devices after the bond pad metalization are shown in Fig(4.6).

4.3.6 Lapping and thinning

The efficiency of a laser device depends critically on the quality of the reflecting edges. The better the quality of the mirror the lower the scattering losses and the higher the lasing efficiency. To get good quality mirrors a perfect cleavage of the substrate is required. A perfect cleave is only possible if the substrate is sufficiently thin such that small nicks made at the edges of the substrate result in the wafer breaking clearly along its natural cleavage planes. It is therefore essential to fabricate the laser devices such that they are aligned along the sample's natural cleavage planes. Lapping of the sample is performed by mounting the sample with Crystal Bond adhesive onto a lapping tool and grinding in a slurry made of silicon carbide (5 μm grain size) and water. The lapping should be performed until the thickness of the sample (monitored by a dial indicator) is reduced to about 100 μm.

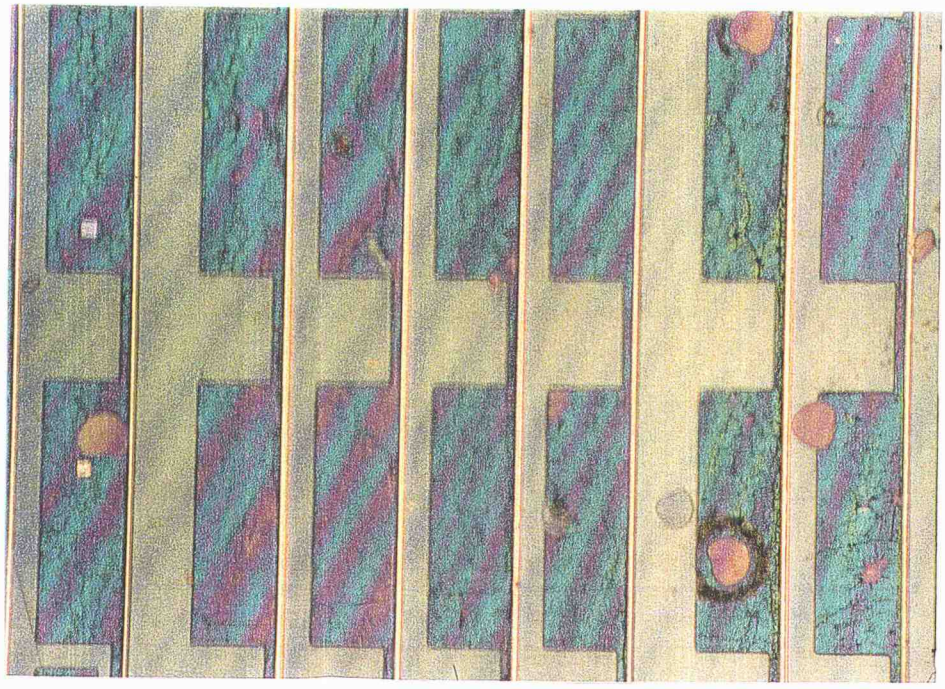

Fig(4.5) Photograph showing completion of level 3 lithography for bond pads.

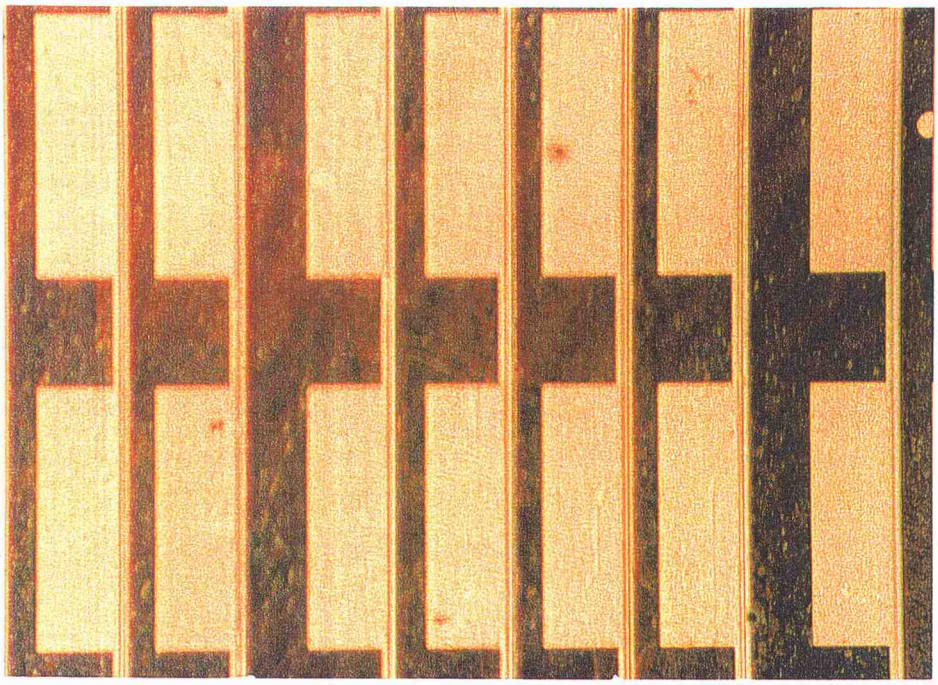

Fig(4.6) Photograph showing devices after gold evaporation.

4.3.7 n-ohmic contact metalization

The n-ohmic contact metal is deposited on the back side of the wafer after the thinning process using the following procedure:

1) Clean the sample by the AMD process.

2) Evaporate n-ohmic metals: 100 Å Ni/500 Å AuGe/1500 Å Au.

3) Anneal the ohmic metals using thermal annealing at 450 °C for 3 minutes.

4) Evaporate 250 Å of Ti and 350 Å of Ni on the annealed n-ohmic metal.

5) Dip the sample in a solution of gold potassium chloride kept at 90 °C for 10 minutes. This would plate about 25 kÅ of electroless gold.

4.3.8 Cleaving, mounting and bonding

The laser devices are subsequently cleaved into small die each of which contain a set of small laser stripes of different widths. The cleavage is initiated by small nicks using a diamond knife edge. The cleaves are made along the stripes at first and then across at right angles. The cleaves made along the stripes are spaced at 200 µm and the cuts across are spaced at various lengths from 0.3 mm to 1 mm. The cleaves are made by allowing the diamond edge to drop gently under its own weight onto the edge of the wafer producing nicks on the edges. When both directions have been marked gently roll a light cylindrical object like a pencil on top of the sample with sufficient cushioning in between the sample and the object. Small die are obtained when the substrate cleaves along the nick marks.

Carefully separate each die and store in an environ free of static charge as the devices are too small to sustain the damaging effects.

Mounting of the devices is done on a special gold plated copper triangular header to provide efficient heat sinking. A die is then mounted on top of the header such that the p-ohmic metal stays on top and the n-ohmic metal is attached to the header with indium alloy solder. The alloy used for this purpose has a composition of 63% tin and 37% lead. The melting point is 183°C. The solder is applied sparingly on the header and the header heated so that the solder melts at 183°C. The die is then gently placed onto the molten solder, pressed down for a thin bond, and the header then allowed to cool down. Extreme care should be taken in placing the die on the header so that the solder does not smear up over the mirror facets. All handling of the laser die must be done in a static-free environment with proper grounding.

Bonding is performed using a wirebonder. Gold wires (.001" thick) are used to bond the top p-ohmic metal contact pads to the external positive contact of the laser driver circuit. This external contact is actually a small pad glued to the metallic header but insulated from it. The metallic header itself is the negative contact for the n-ohmic metal of the laser diode. The bond wires are first bonded to the metal pad for external contact through ball bond. This is followed by a stitch bond on the device. For the devices fabricated in this project, aluminum wires were used because of lack of adhesion between the gold wires and the plated gold pad. Aluminum bonding can be done at room temperature unlike gold bonding, which requires a temperature around 120 °C or more.

The processing steps dicussed in this section are illustrated in Fig(4.7).

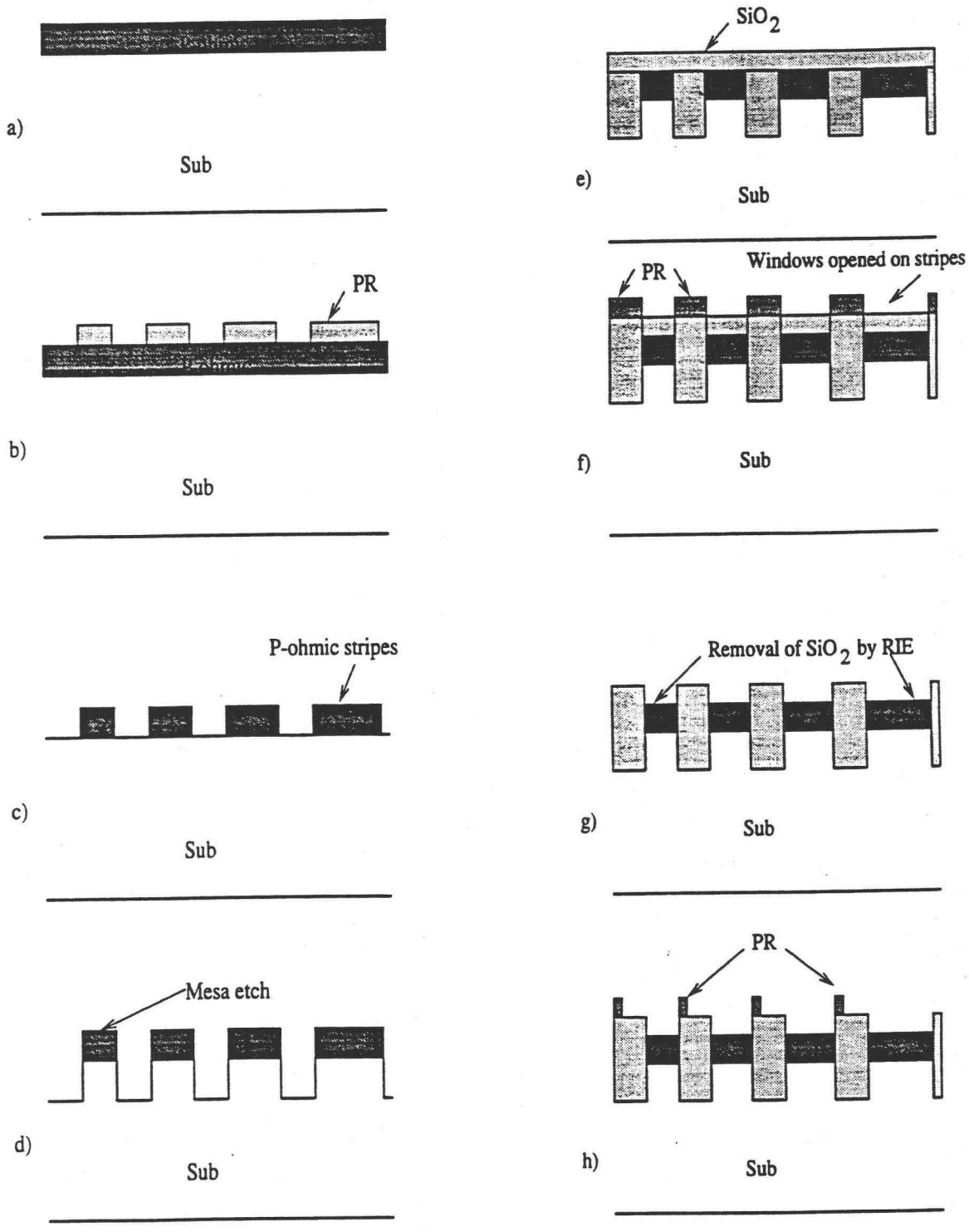

Fig(4.7) An illustration of different steps required for the fabrication of LDs

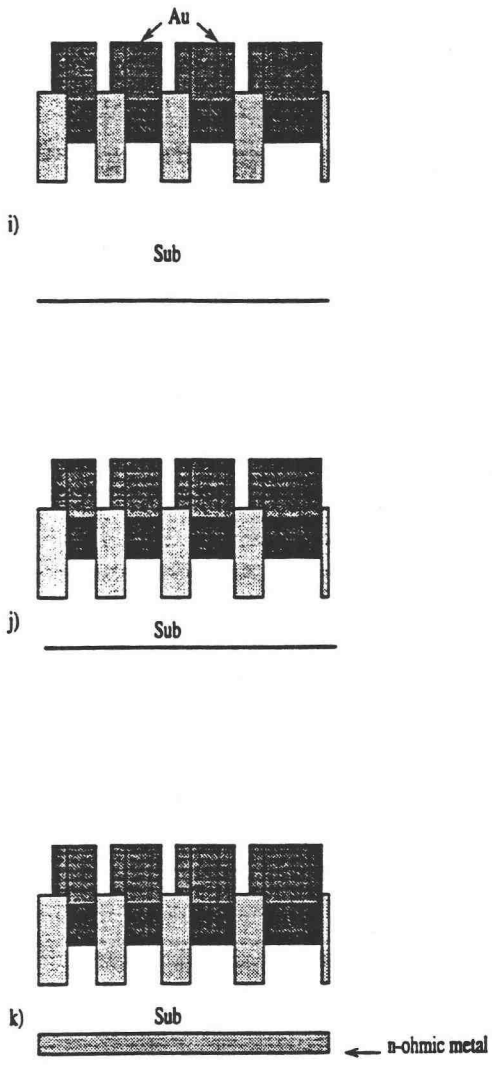

a) Deposition of p-ohmic metal

b) Level 1 lithography: Defining stripe regions.

c) KI/I_2 gold etch.

d) Meas etch.

e) Silicon dioxide deposition

f) Level 2: Opening windows on top of the stripes.

g) Removal of silicon dioxide by RIE and dissolution of PR with solvents.

h) Level 3: Defining contact pads.

i) Contact pad metal lift off.

j) Lapping of bottom surface

k) n-ohmic deposition on bottom surface.

Fig(4.7) Contd.....

5. Electrical and Optical Characterization

5.1 Introduction

The devices after fabrication need to be tested for electrical and optical characteristics. Current-voltage characteristics, light output vs drive current plots and spectral gain characteristics for these devices are determined to verify their electro-optic behavior. The experimental setup required for these tests is briefly described in the section for testing consideration. Also results from I-V, L-I and spectral gain measurements are presented and analyzed. Finally the results are summarized.

5.2 Testing considerations

Devices were tested under room temperature conditions. The most important tests for these devices are the L-I characteristics, I-V curves, and spectral gain characteristics. The test fixture consists of an aluminum heat sink on top of which the header is fixed. A small circuit board is glued down to an insulating block of Plexiglas which also holds the aluminum heat sink. A 10 Ω resistor is used in the circuit to limit and measure the forward current. A diode is also used in the circuit as a regulator to prevent any negative pulses from reaching the laser diodes. This is because the LDs are operated only under forward bias conditions and any reverse bias would have destructive effect on the active region.

The test arrangement is shown in Fig(5.1). Two BNC connectors are provided, one for applying the positive bias and the other for monitoring the diode current. The diodes are first tested under pulsed conditions. Depending on the terminal resistance of the active region, some samples are identified for CW operation. Room temperature measurements are of particular interest to this thesis.

5.3 Results and discussion

5.3.1 I-V results and analysis

I-V measurements were performed using an HP4145B parameter analyzer. A voltage in the range of 0 V- 2.0 V was swept across the contacts and the current plotted on the y-axis. The turn-on voltage observed for the diodes of widths 4 μm, 6 μm, 8 μm and 10 μm was near 1.35 V. The forward current was found to be in the range from 5mA for the 4 μm wide stripe to about 14 mA for the 10μm wide stripe. The current values for the 6 μm and 8 μm wide stripes were found to be 7 mA and 12 mA respectively. These results are consistent with theory that diodes with greater active area would need larger amounts of forward current. The diodes were mounted on the heat sink and the I-V measurements were repeated. A forward current of about 40 mA was obtained for a forward bias in the range of 0 V to 2 V as seen in the I-V plots. The turn-on voltage remained at 1.35 V approximately. These results are confirmatory tests for the diode behavior of the mounted devices, on which further tests like L-I analysis, spectral gain etc. would be performed. An infra-red viewer was also used to visually examine the facets

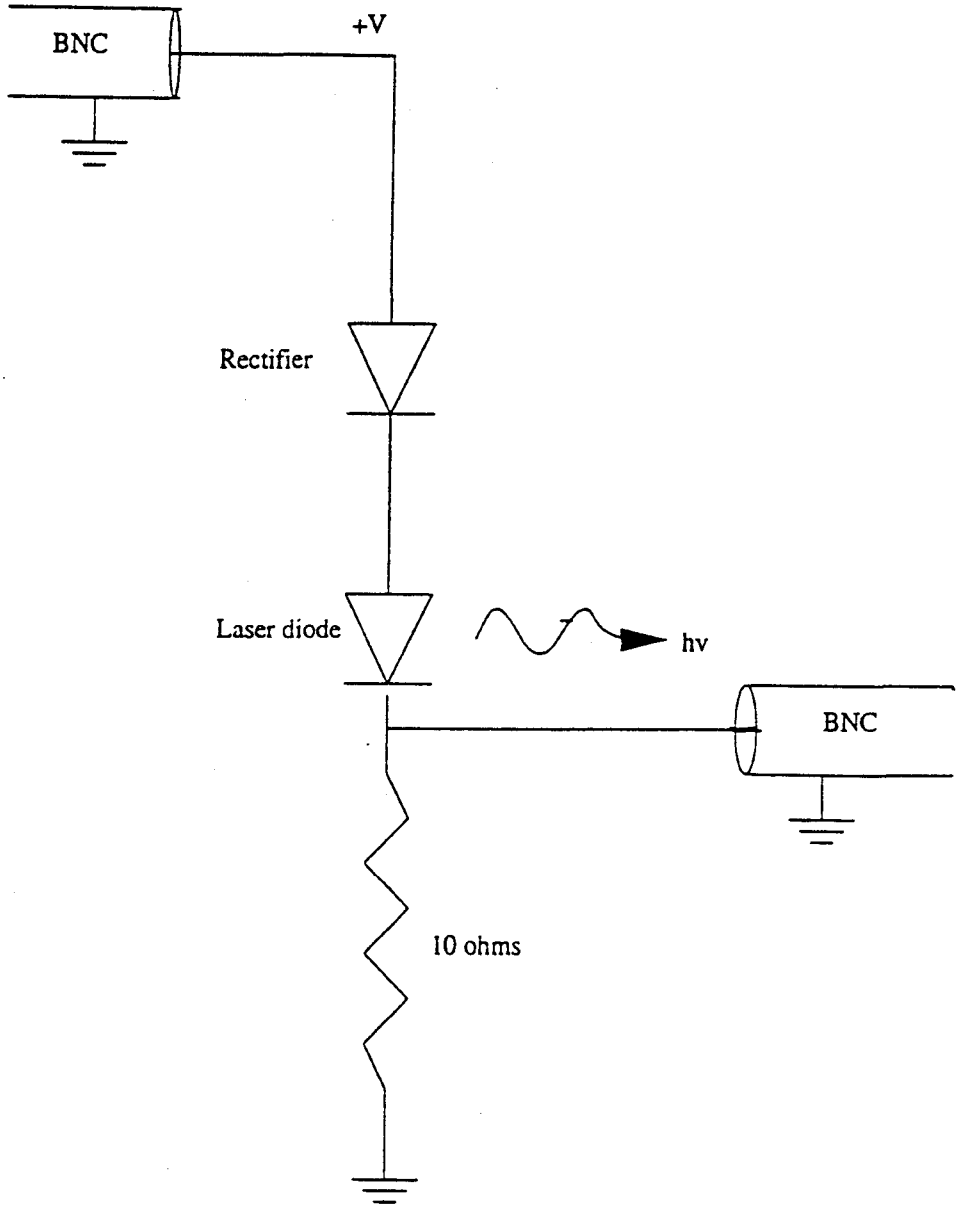

Fig(5.1) Test circuit for laser diodes.

of the devices during the I-V measurements to detect any light generated. It was possible to see clearly the emergence of light from the facets as soon as the laser diodes started turning on at 1.35 V. The turn-on voltage of 1.35 V corresponds closely to the 1.422 eV bandgap of the GaAs active layer at 300K with low minority carrier injection. Figures (5.2) through (5.5) show the I-V and Log(I)-V plots of the 8 μm wide MBE and MOCVD LDs.

In order to verify the I-V characteristics of the LDs fabricated, I-V measurements of a commercial laser device, made by Sharp Co. and having peak emission wavelength of 780 nm, were taken. The I-V results of this laser (LT027) are shown in Fig(5.6) and Fig(5.7). The semilog plot of the I-V characteristics indicates an ideality factor of approximately 1 over three decades (190 mV over three decades) of current. After this the series resistance takes over. Compared with these results the semilog plot of the I-V characteristics of the MBE and MOCVD LDs fabricated for this research indicates an ideality factor of 2 over three decades of current. Since ideality factor is a direct measure of the ideal conditions during device fabrication, from the above results it can be deduced that the LDs fabricated for this research are not as close to ideal as the commercial diode.

Fig(5.8) shows the band diagram of a GRIN-SCH double heterojunction laser diode under forward bias conditions. It can be seen that the barrier height across the undoped GaAs active region is reduced due to the forward bias voltage V_f, such that holes from the p-AlGaAs and electrons from the n-AlGaAs layers overcome the barrier and start filling the valance and conduction bands respectively. Radiative recombination thus occurs

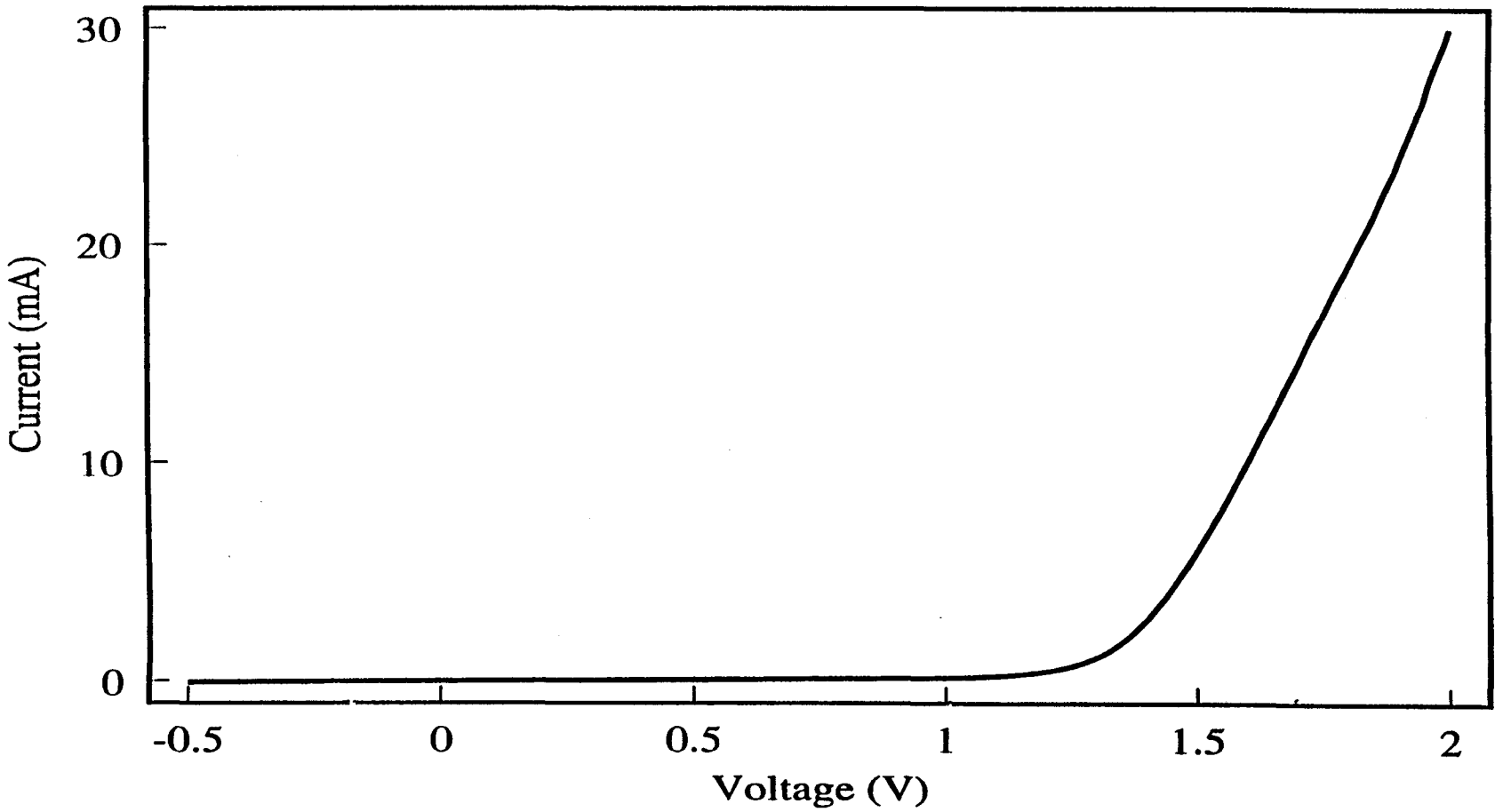

Fig(5.2) I-V of 8μm wide MBE laser.

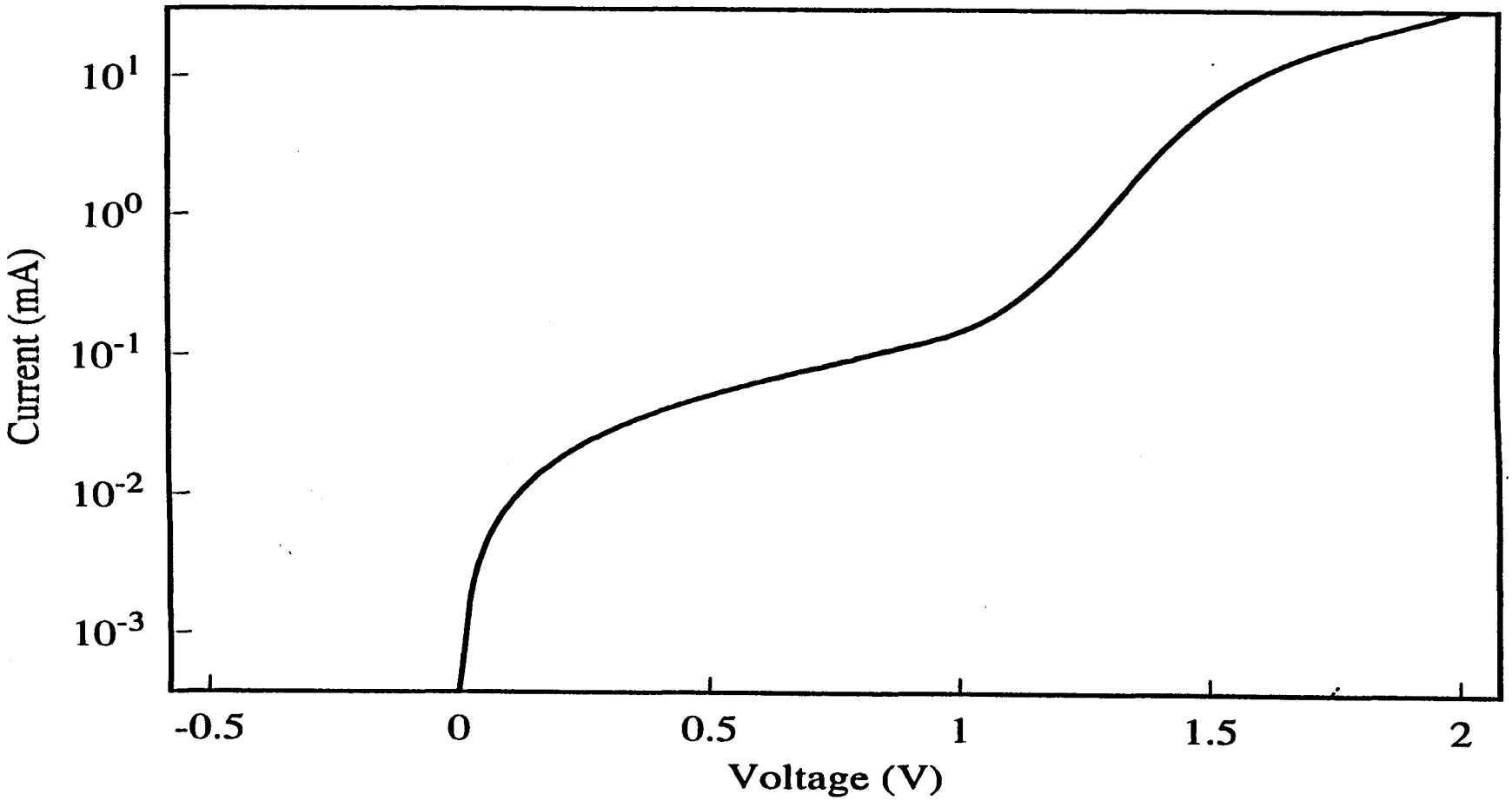

Fig(5.3) Log(I)-V of 8μm wide MBE laser.

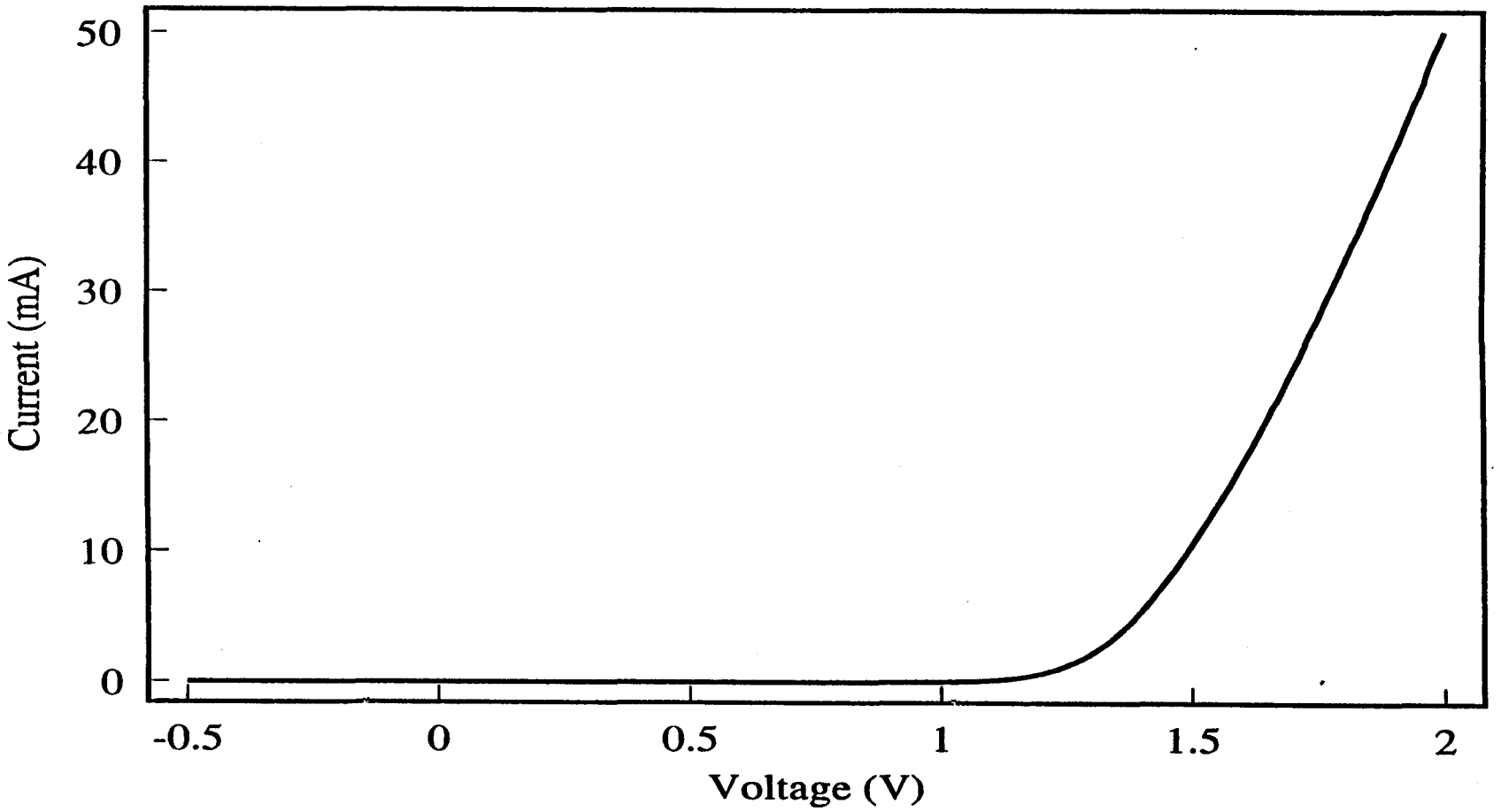

Fig(5.4)characteristic of 8μm MOCVD laser mounted on heat sink.

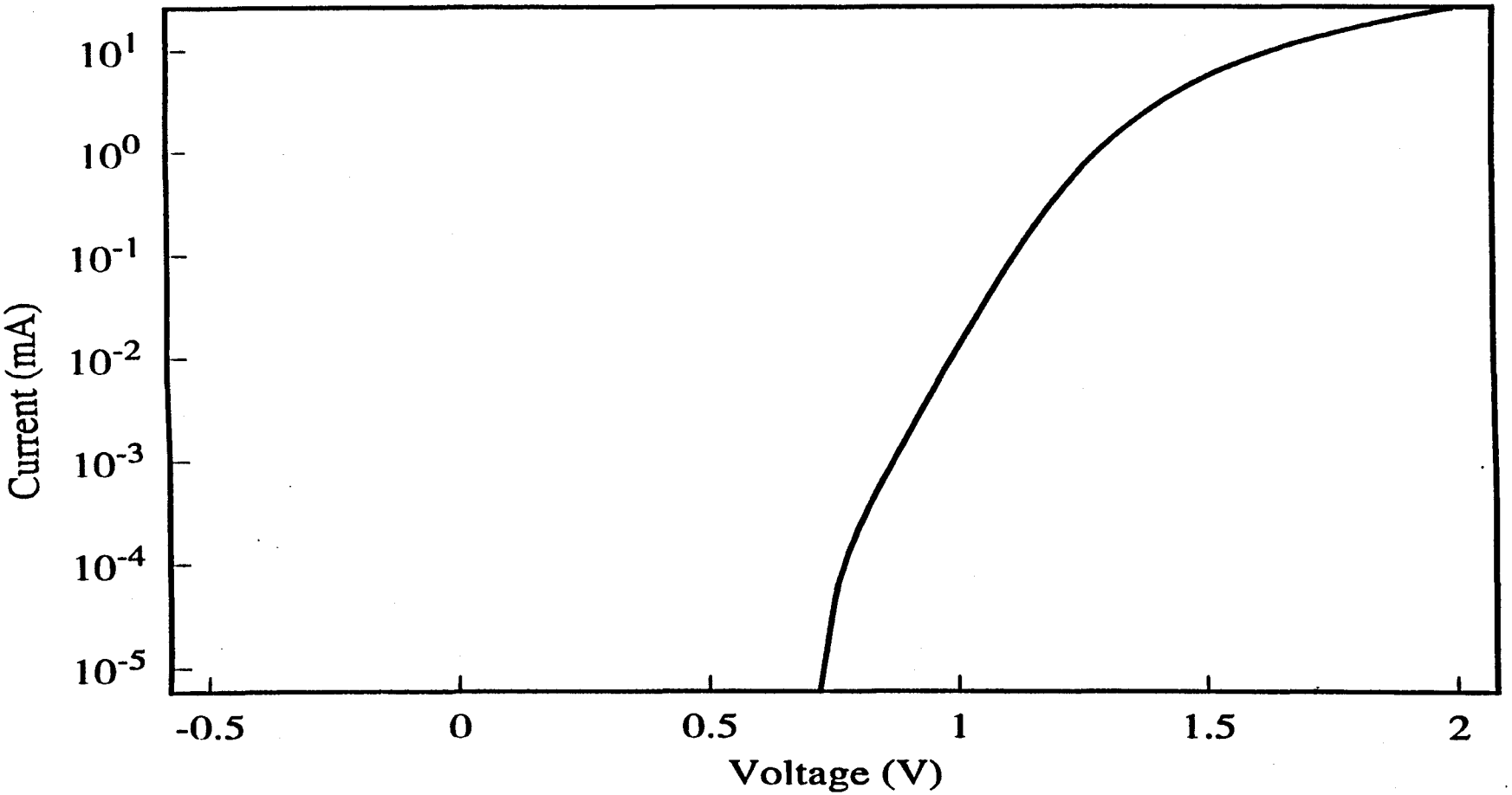

Fig(5.5) Log(I)-V characteristics of 8μm wide, MOCVD laser mounted on heat sink.

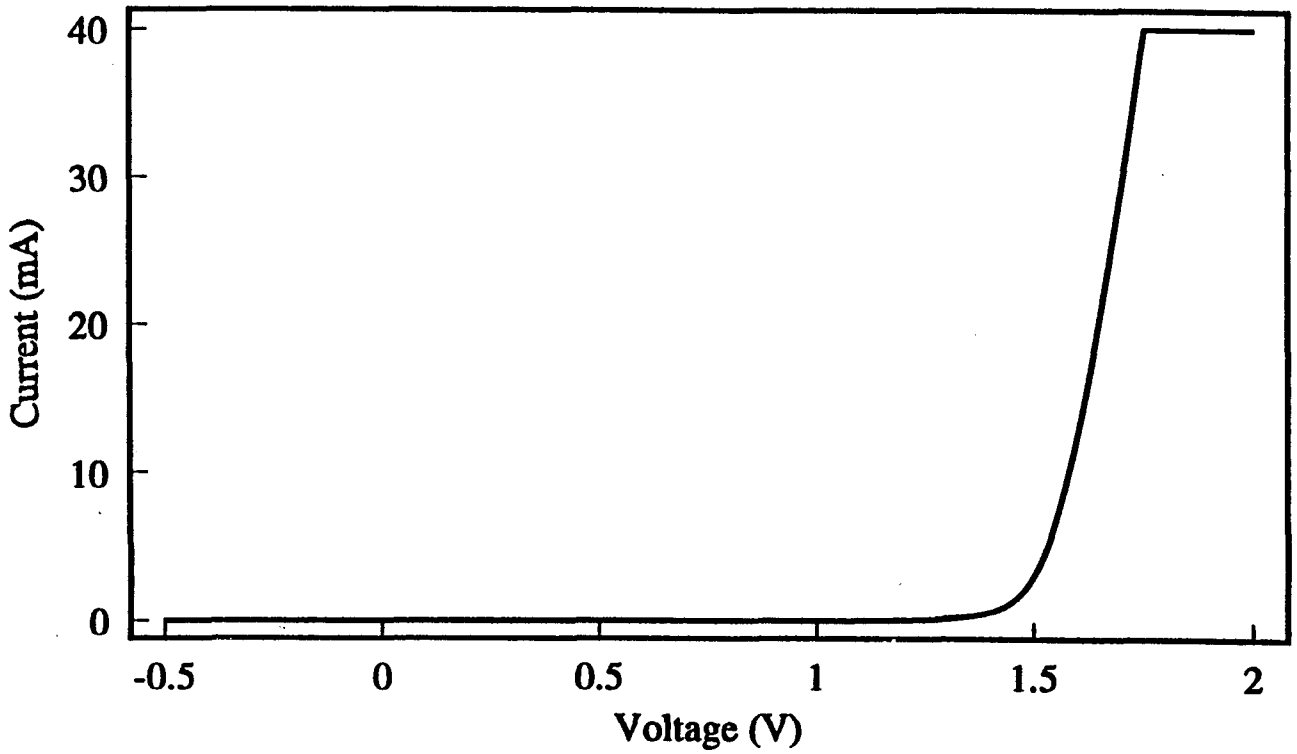

Fig(5.6).I-V of a commercial diode (Sharp LT027MD)

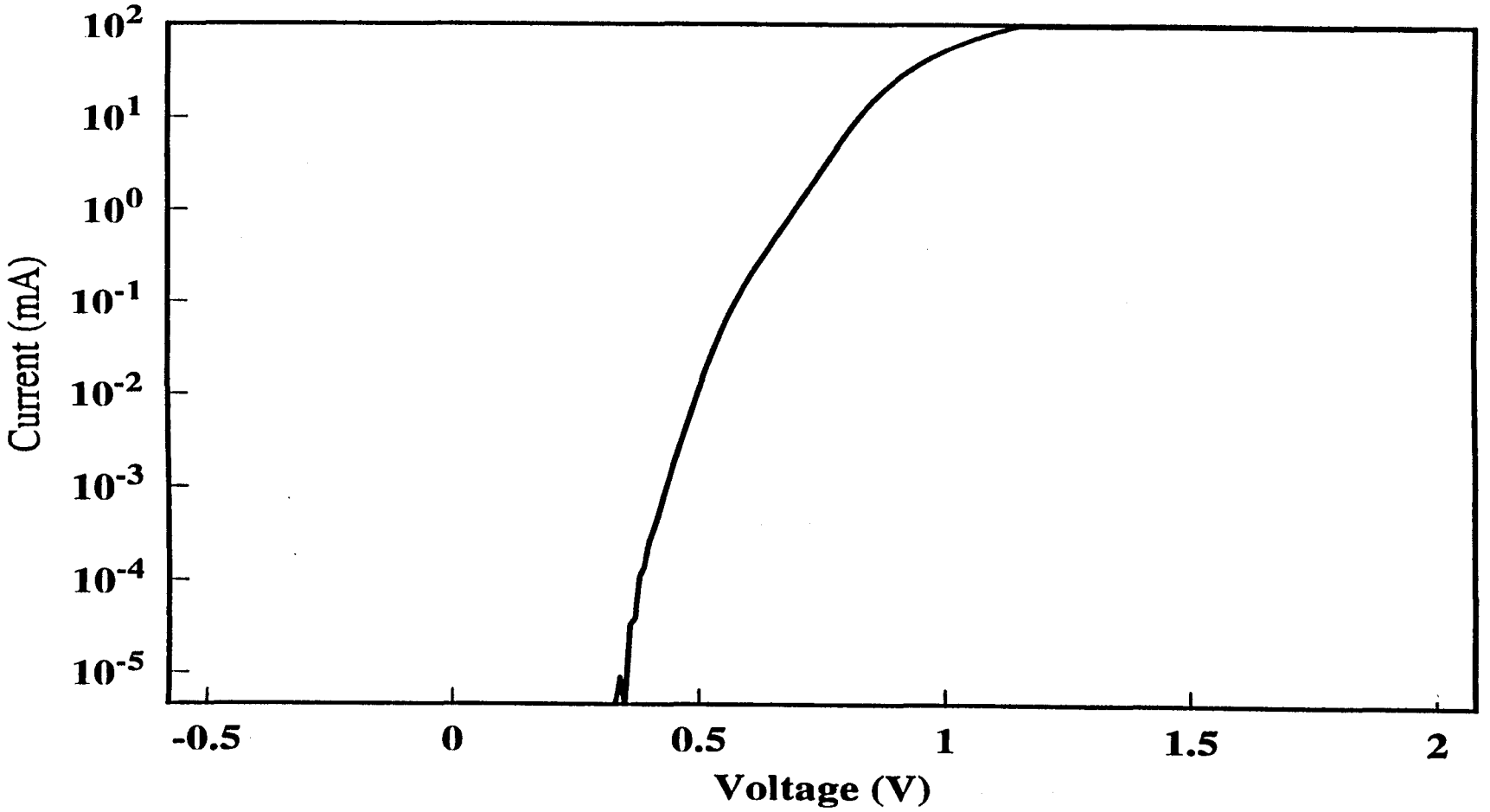

Fig(5.7) Log(I)-V of commercial diode.(Sharp Corp. λ=780nm)

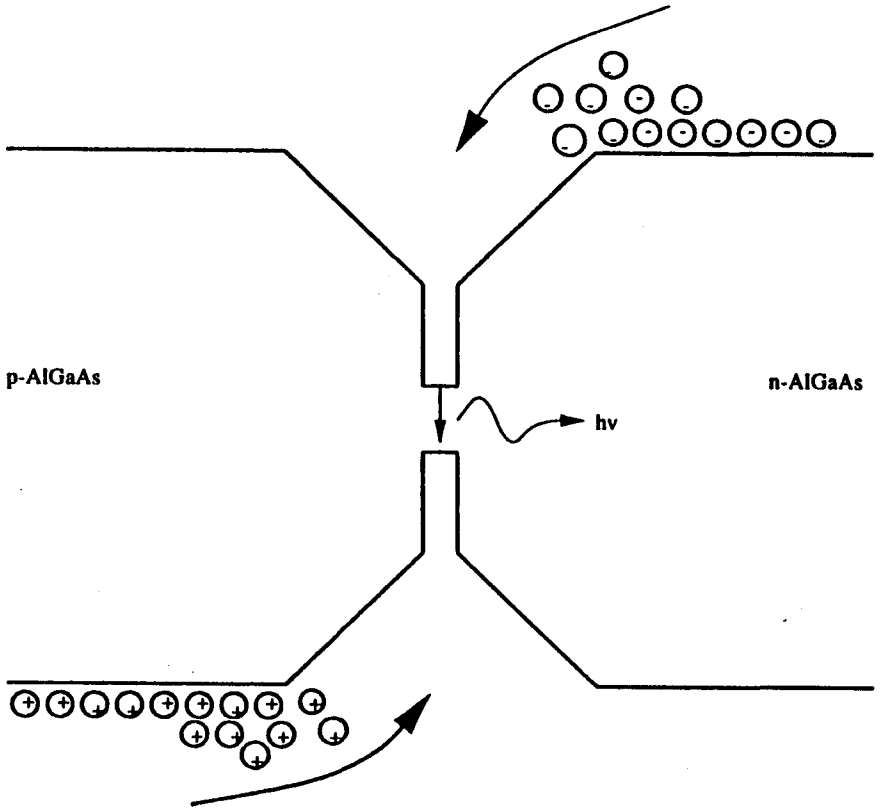

Fig(5.8) A GRIN-SCH structure under high forward bias.

in the active region when the electrons relax to the ground state and lasing can be attained by maintaining some kind of pump mechanism as elaborated in chapter 2.

5.3.2 L-I results and analysis

The light-output plotted against the drive current is a good method of estimating the threshold current and quantum efficiency of a laser diode. A typical L-I plot of a LD shown in Fig(5.9) displays a low slope linear region for lower current levels which represents the spontaneous emission regime of the LD. This is followed by a sharp increase in slope as the current level approaches threshold when the LD enters the stimulated emission regime. The threshold current is found by the extrapolation of the curve to the current axis. Also the differential quantum efficiency (in mW/mA) of the LD is determined by the slope of the L-I curve in the stimulated emission regime. The L-I plot of the commercial diode (Sharp, LT027MD) is shown in Fig(5.10). The threshold current is 35 mA and differential Q.E is 0.382 mW/mA. These values are in very close agreement with the specifications provided by the supplier (I_{th} = 35 mA, η_{diff} = 0.35 mA/mW). This verifies the correctness of the L-I experimental setup.

The L-I characteristics of the MOCVD and MBE lasers, 500 μm long, are shown in Figs(5.11) through (5.13). For the 10 μm wide MOCVD LD the threshold appears to be about 190 mA (J_{th} = 3.8 kA/cm^{-2}). The maximum power derived from this device was about 1.1 mW when the device started deteriorating rapidly. Differential Q.E in the stimulated regime, determined from the plot is 0.011 mW/mA. The 8μm MOCVD laser

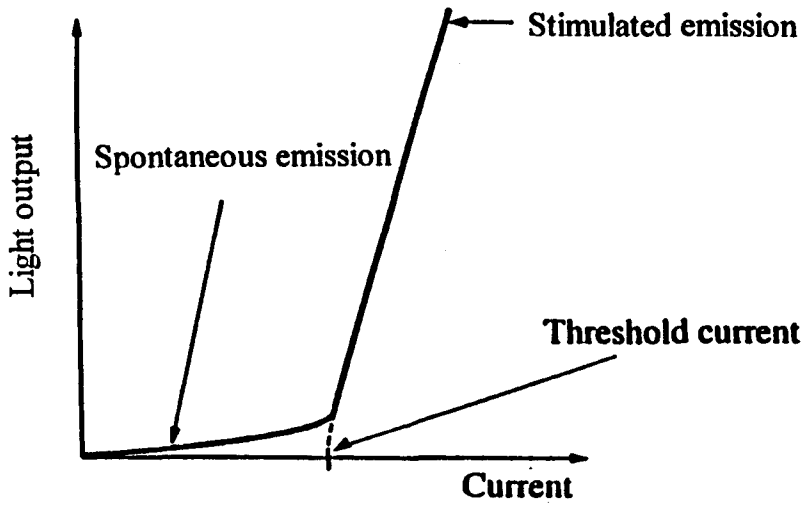

Fig(5.9). Light output-current characteristic of an ideal semiconductor laser

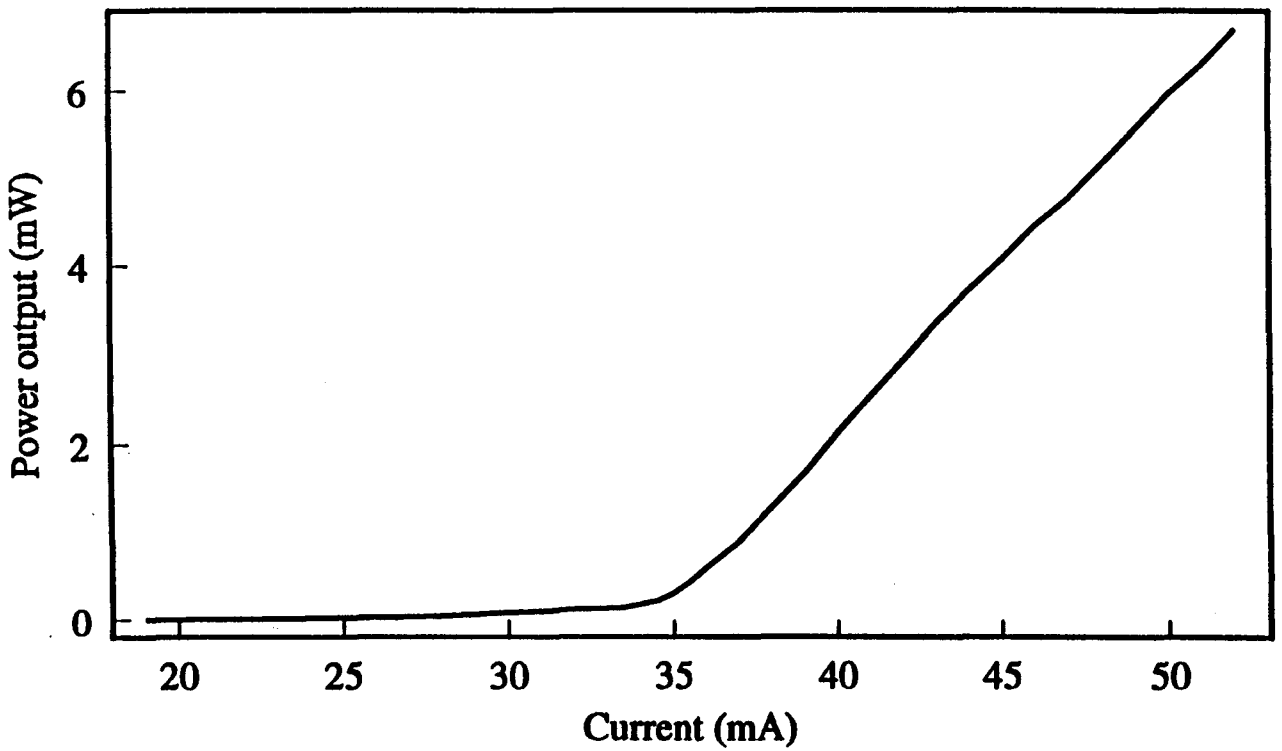

Fig(5.10) L-I of Commercial laser diode(LT027MD0, Sharp)

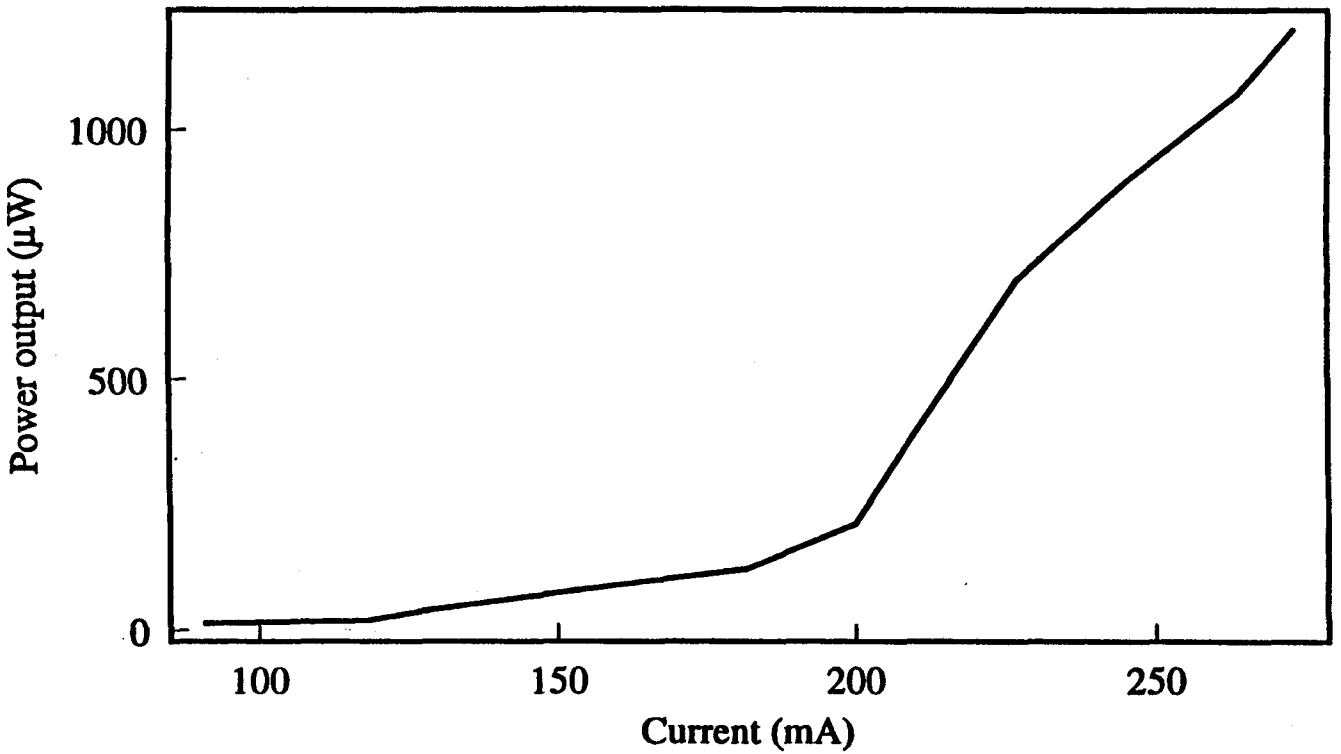

Fig(5.11).L-I plot of MOCVD 10μm wide laser.

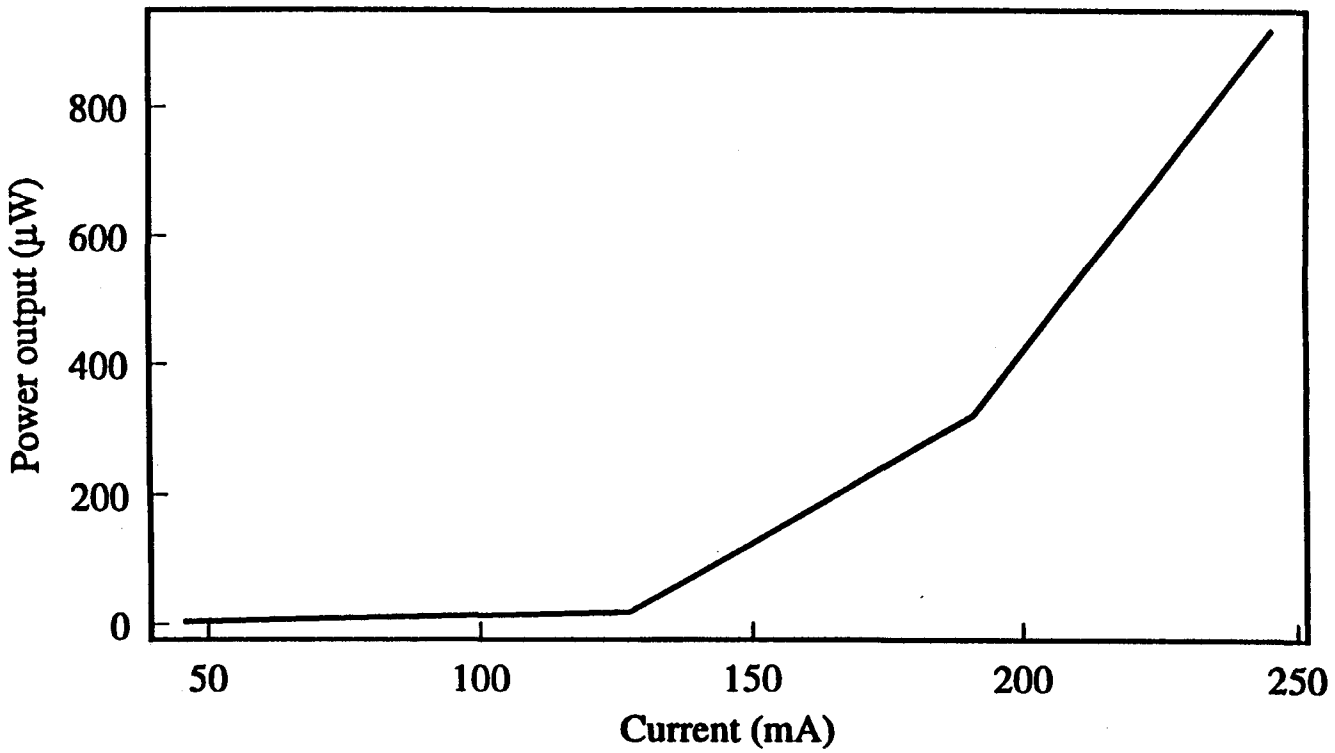

Fig(5.12).L-I plot of MOCVD 8μm wide laser.

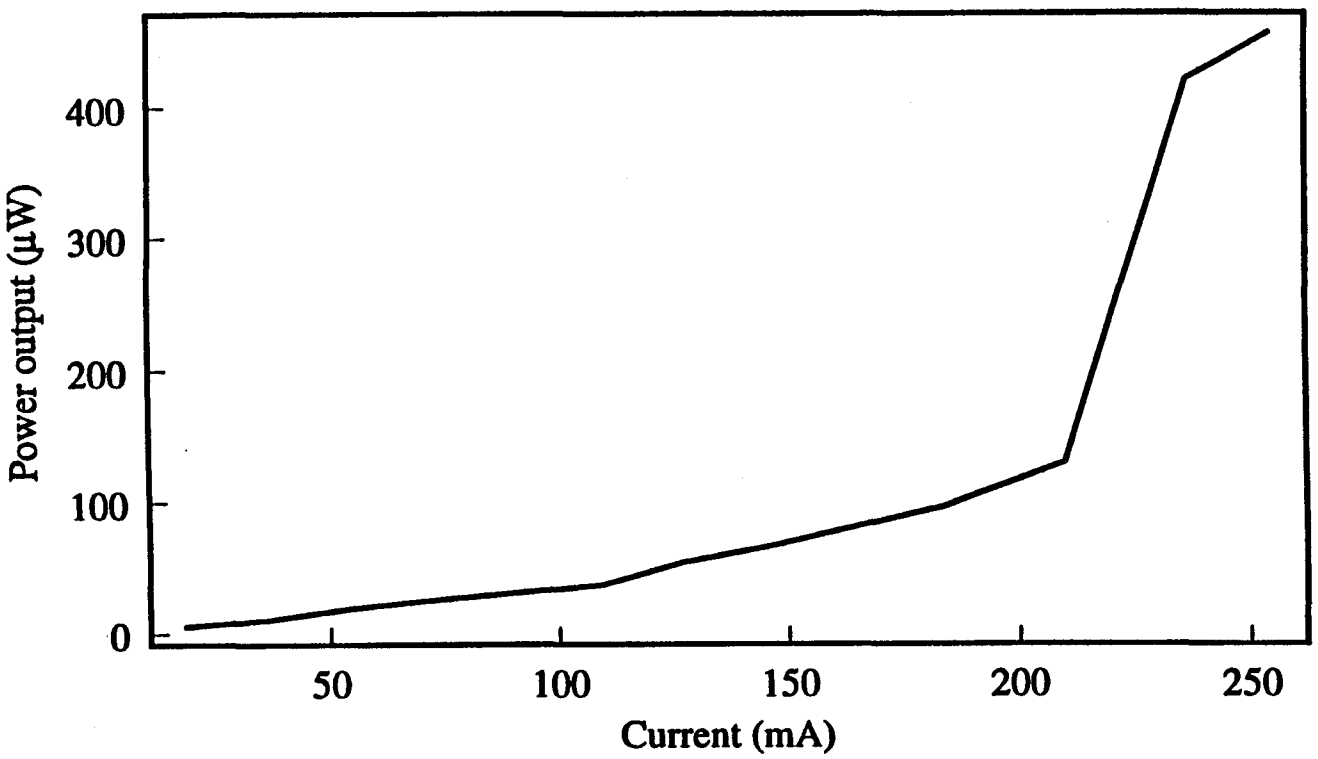

Fig(5.13).L-I plot of MBE 10μm wide laser.

exhibits a threshold of 160 mA (J_{th} = 4 kA/cm^{-2}). The differential Q.E is 0.006 mW/mA. This is about 45% lower than that observed for the 10 μm wide laser. The lasers made for this thesis are index guided and hence carrier confinement is mainly determined by the area of the stripe. Since the 8 μm laser has less area than the 10 μm laser its output power can be expected to be lower.

The L-I plot for a 10 μm wide MBE laser (Fig 5.13) shows a threshold current of 200 mA (J_{th} = 4 kA/cm^{-2}) and a differential Q.E of 0.012 mW/mA. This is in good comparison with the figures for the 10 μm MOCVD lasers. The output power for this device as compared with the similar geometry MOCVD device is roughly half. This does not necessarily reflect the quality of the MBE material. Further comparisons of similar geometry devices on both these materials should be done in order to determine the quality of the MBE for effective use in laser fabrication.

5.3.3 Spectral results and analysis

Room temperature spectral measurements are performed with the LDs operated in pulsed mode with 2.5% duty cycle square wave pulses. A setup similar to the PL experiment setup is used. The synchronous output trigger from the pulse generator is used as an input trigger to the lock-in amplifier. A 0.5 m Jarrel Ash monochromator is used to scan the light output from the LDs. Normal grating is used in the monochromator and the slit width is kept at 10 μm. The PMT voltage is kept in the range of 800 V to 1000 V. A

slow scan speed is desired for good resolution of the modes in the output spectrum and a rate of 50 Å/min. is the slowest rate possible in this system.

To calibrate the system a commercial laser diode (LT027. Sharp Corp.) with I_{th}= 40 mA and $\lambda_{peak} = 780 \pm 15$ nm is used. Spectral output from this LD is shown in Fig(5.14). Peak emission above threshold is obtained at 789 nm and a FWHM of 2 Å. These results are within the range as specified by the manufacturer and also confirm that the system is calibrated properly.

Spectral plots of the 500 μm long MOCVD LDs of stripe widths 10 μm, 8 μm and 6 μm, and operated above threshold, are shown in Figs(5.15-5.18). The 10 μm wide LD has a peak at 8370 Å and a FWHM of roughly 2 Å when driven above threshold (1.2 I_{th}) at 228 mA. Another peak of half intensity is also observed at 8378 A°. It could be possible that the LD is barely lasing and that the drive current is still insufficient for the LD to operate far into the stimulated regime. A plot showing below threshold operation of this LD displays a very broad, modulated spectrum with peak at about 8320 Å and a FWHM of 175 Å. This is quite expected of the LD which behaves as an LED when operated below threshold. The spectral plot of the 8 μm wide MOCVD LD shows a peak emission at 8360 Å and a FWHM of 4 Å when driven at 1.5 I_{th} (240 mA). The peak intensity is comparable with that of the 10 μm wide LD but theoretically the output intensity for the 8 μm wide LD is expected to be higher than that of the 10 μm wide LD. This is because the threshold current density for the 8 μm wide laser is less than that for the 10 μm LD and also the output power P_{out} varies directly as J - J_{th}. In line with the

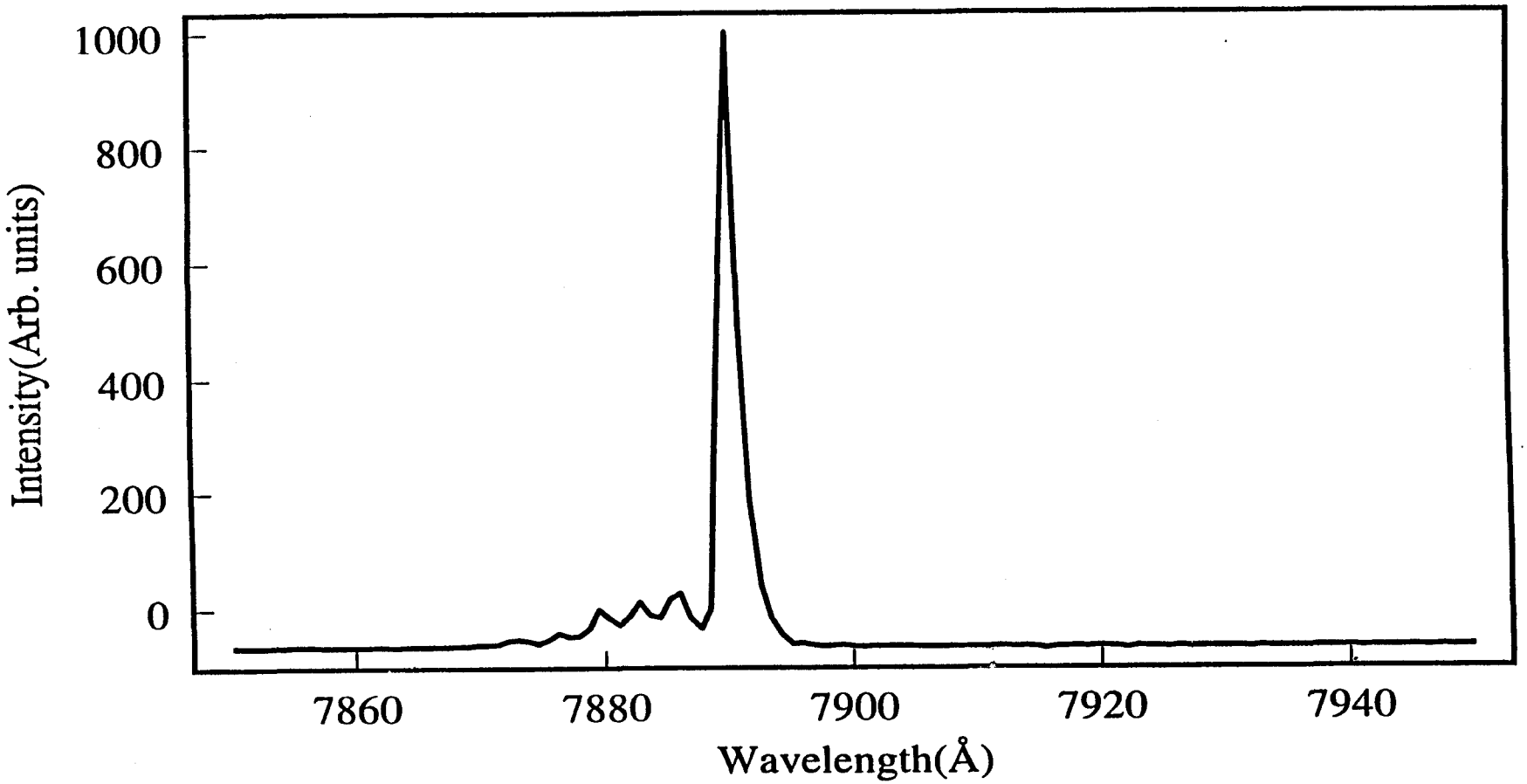

Fig(5.14) Spectral gain curve of commercial laser diode, λ(peak)=789nm

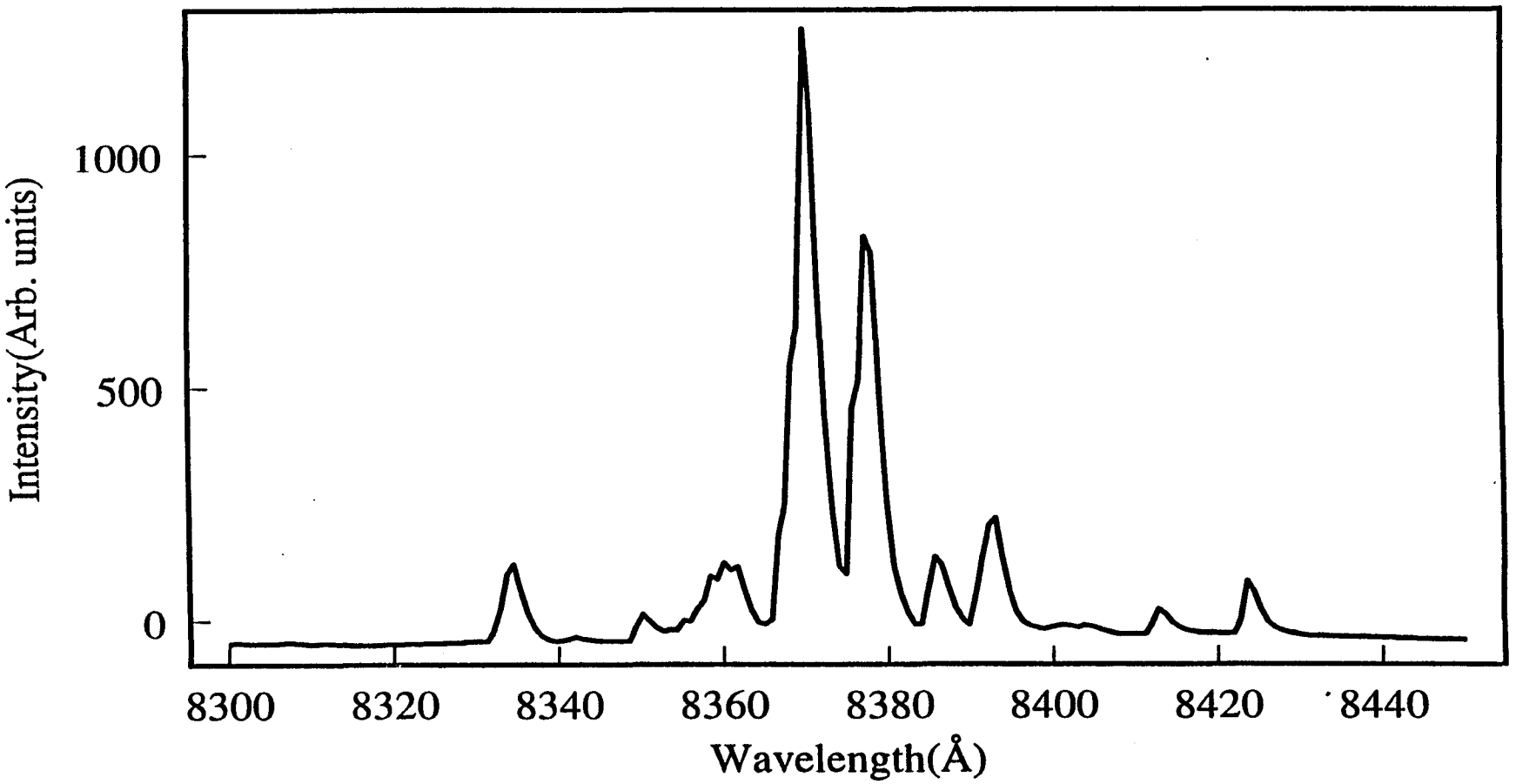

Fig(5.15) MOCVD Laser having 10μm wide stripe and operated above threshold (1.2Ith)

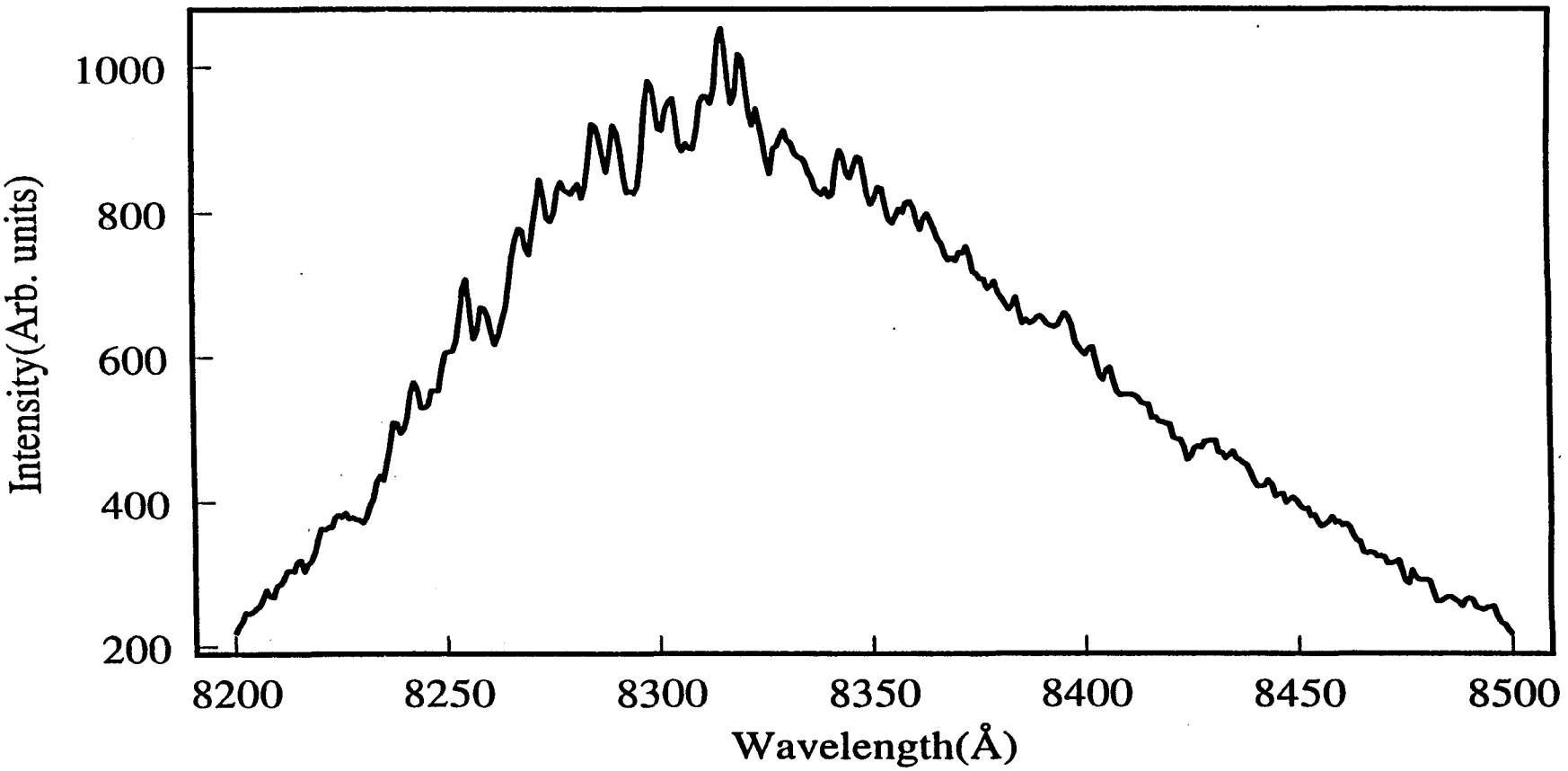

Fig(5.16) MOCVD Laser having 10μm wide stripe and operated below threshold (0.5Ith)

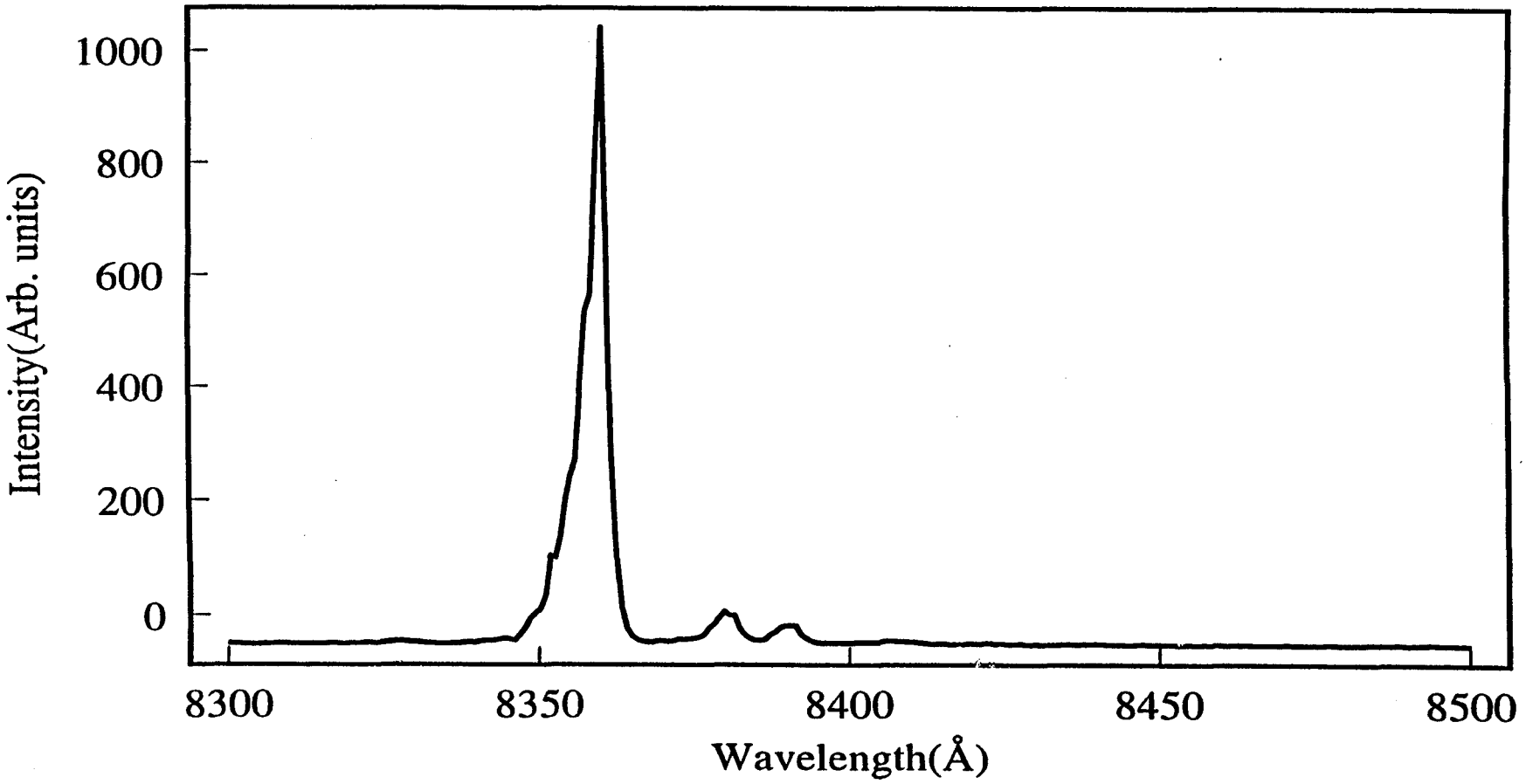

Fig(5.17) MOCVD laser having 8μm wide stripe and operated above threshold (1.5Ith)

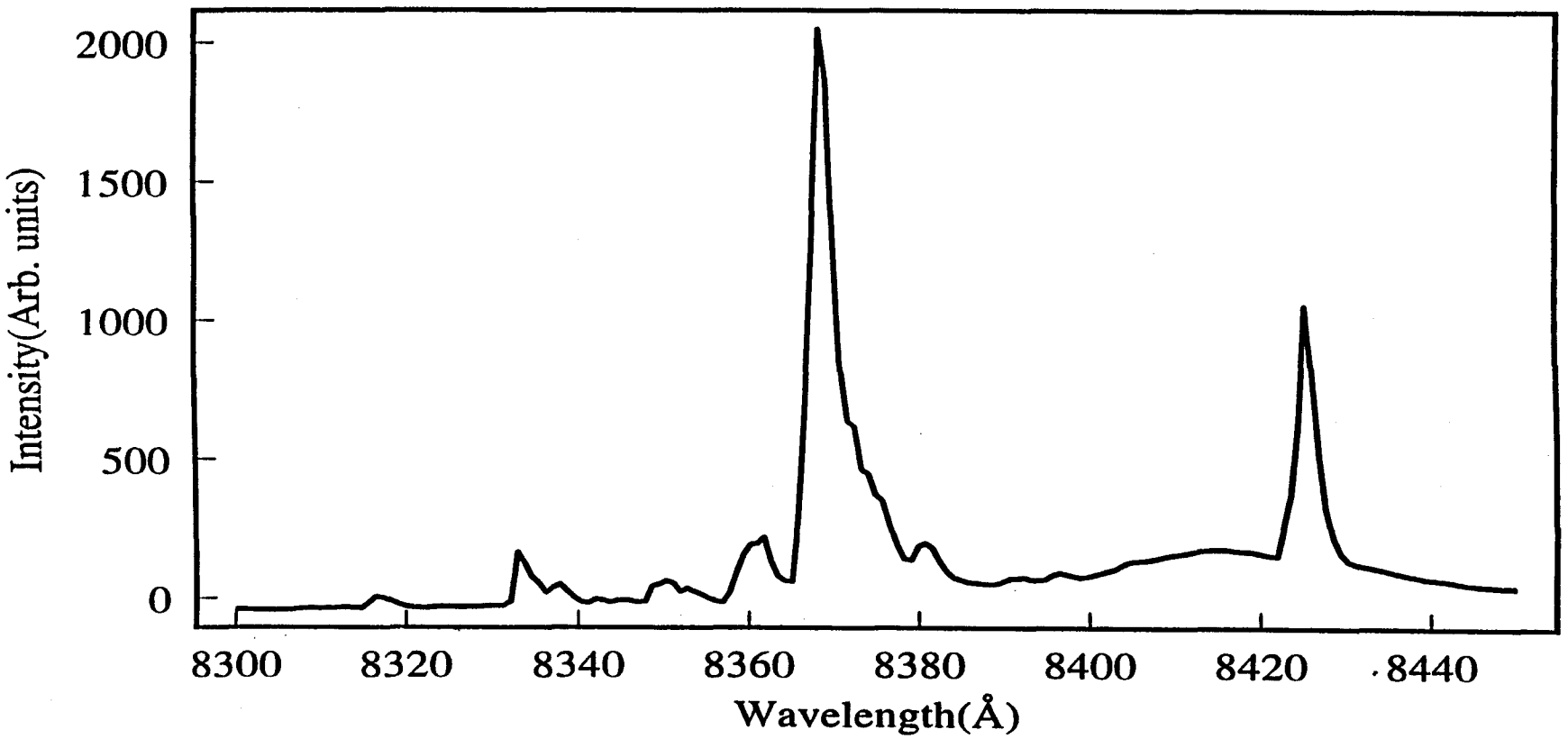

Fig(5.18) MOCVD Laser having 6μm wide stripe and operated above threshold (1.2Ith)

above arguments the spectral plot of the 6 μm wide LD has a peak 8370 Å with twice as much intensity as the other two LDs. This is definitely in agreement with theory. The 4 μm wide LDs did not emit appreciable amount of light and they were mostly having LED like characteristics. This is an anomalous behavior as this LD can be expected to lase at a much lower threshold. The only possible explanation for this behavior could be that the narrow width of the long stripes might have caused significant undercutting of the 4 μm wide stripes during processing. This can result in either a complete loss of the p-ohmic metal stripe from different regions of the substrate or a poor contact of the metal stripes with the mesa resulting in less number of carriers reaching the active region.

The 10 μm wide and 500 μm long MBE LD displayed a peak at 8165 Å with a FWHM of 2 Å as shown in Fig(5.19) and Fig(5.20). The intensity is half as much as compared with the same width MOCVD LD. The lasing wavelength is also significantly lower than the peak wavelength of the MOCVD LD. For GaAs quantum well lasers the peak emission wavelength is expected to be lower than that of bulk GaAs (873 nm approx. at 300 °K) due to quantum confinement effect which results in an increase in the energy of the radiative emissions. Since in this case the peak emission wavelength is much lower than the peak wavelength of the MOCVD LD it is most likely that the quantum well width of the MBE material is less than the designed thickness of 58 Å. This in turn might have been caused due to variations in growth parameters during MBE growth. When operated below threshold this device showed a wide spectrum with FWHM of 150 Å. Spectral measurements of the 8 μm, 6 μm and 4μm MBE lasers did not reveal any appreciable output. This again could be attributed to the processing limitations mentioned earlier in

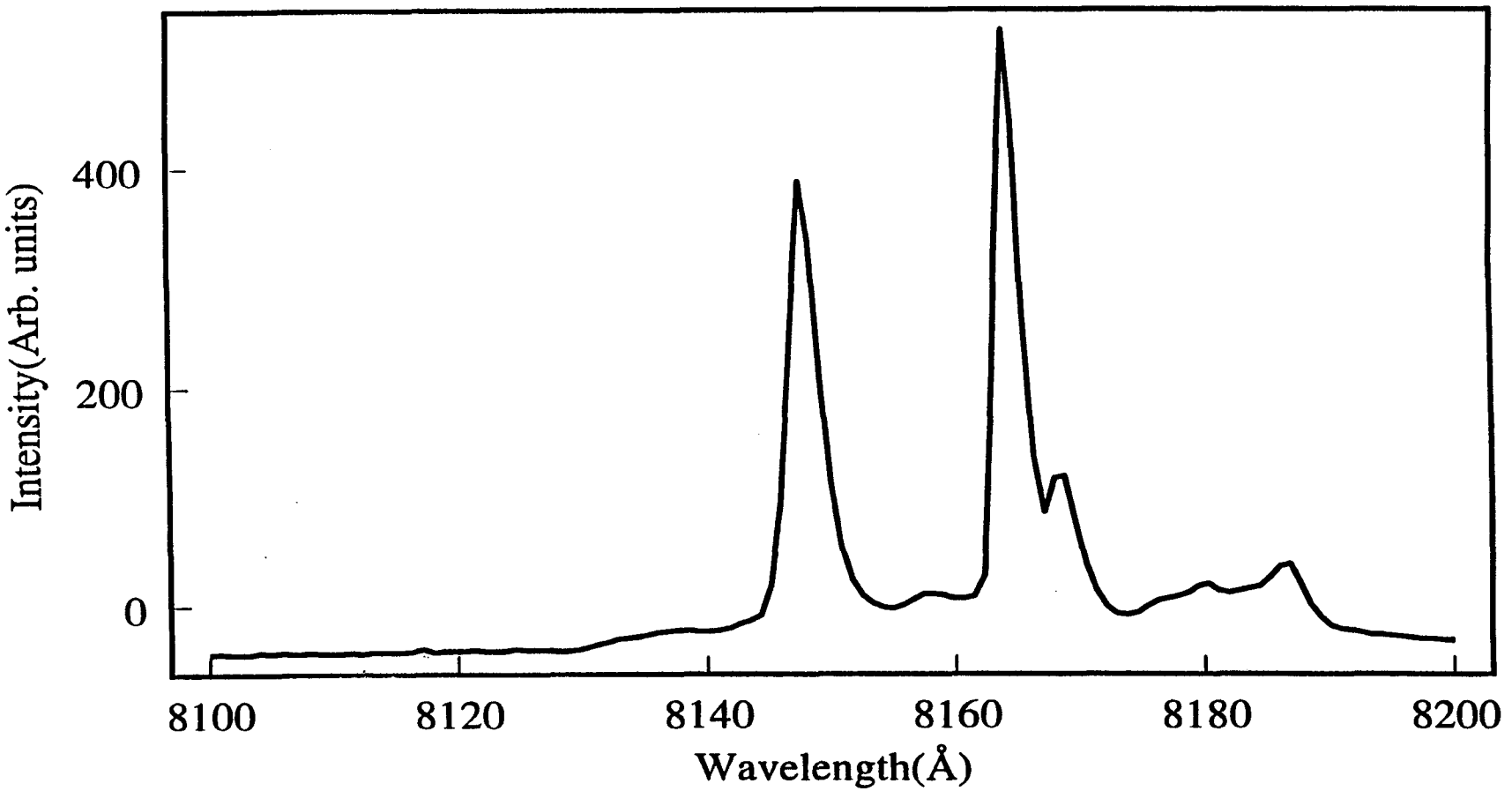

Fig(5.19) MBE laser having 10μm wide stripe and operated above threshold (1.2Ith)

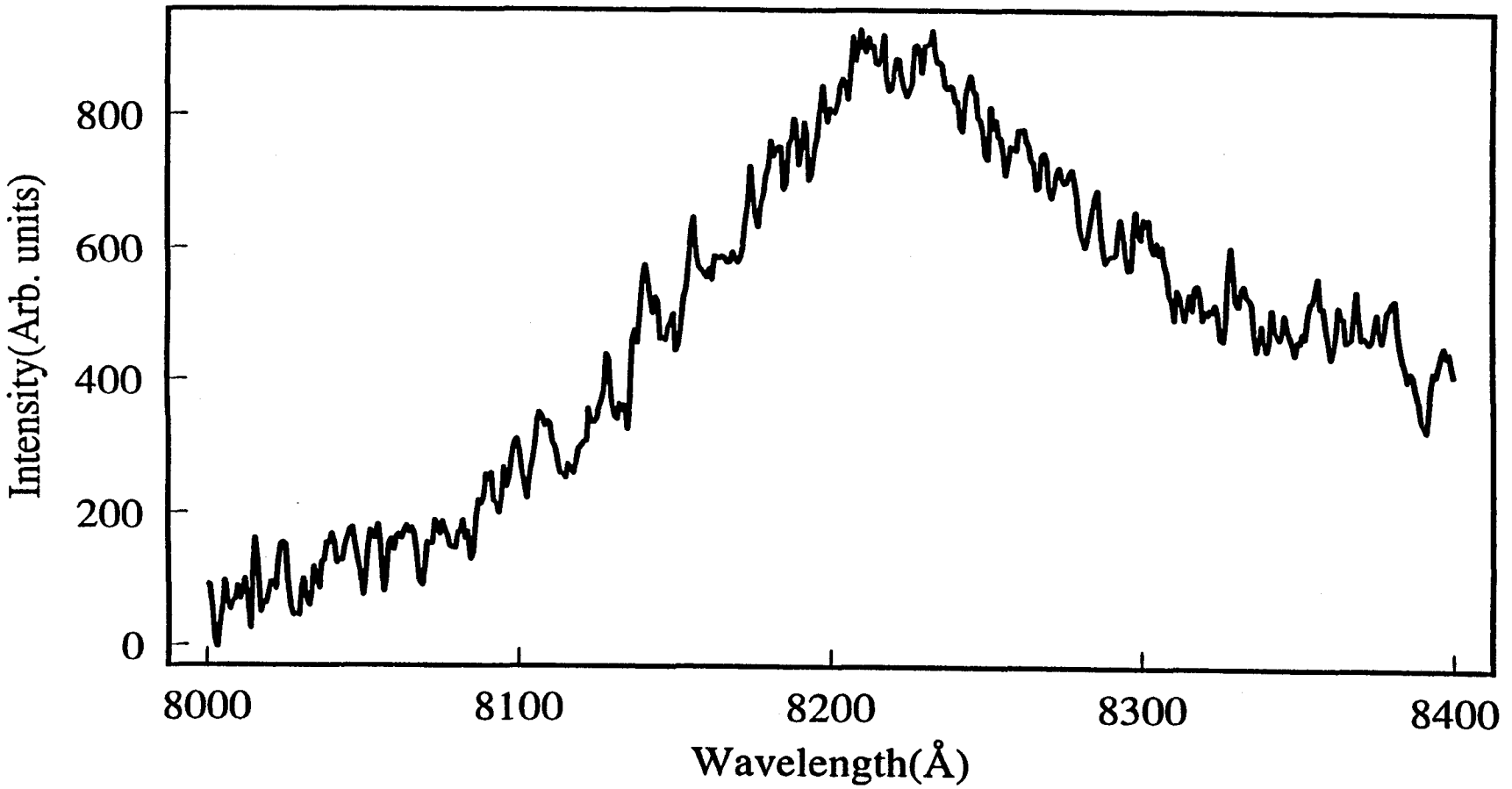

Fig(5.20) MBE laser having 10μm wide stripe and operated below threshold (0.5Ith)

this section. It is also possible that minor defects noticed on the cleaved mirrors contributed to huge losses at the end facets. Apart from this, scattering loss due to scattering of the propagating modes out of the active guiding region by dielectric or heterostructure imperfections or coupling loss, which results from the optical modes spreading beyond the wider energy gap cladding layers can be held responsible for the poor output from these devices.

5.4 Summary

The electrical and optical measurements were calibrated using a commercial LD made by Sharp Corporation. Specifications for threshold current, differential quantum efficiency, spectral gain etc. were satisfied. The I-V results for the diodes on both the materials shows a turn-on voltage of 1.35 V. Ideality factor is found to be twice as bad as the commercial diode. L-I plots indicate that the threshold currents and threshold current densities for the devices of similar dimensions on both the materials are comparable. After comparing three devices each of the MBE and MOCVD material it is found that the output power of the MOCVD LD is twice as much as the MBE LD. Spectral gain plots show that the MOCVD LDs lases in the 830 ± 20 nm range, as specified by the manufacturer. The MBE material though appears to be lasing at a much lower wavelength (8150 Å) indicating that the width of the quantum well is less than originally designed.

6. Conclusions and Future Scope

6.1 Summary and conclusions

This thesis reports on the material and device characteristics of 830 nm diode lasers fabricated on MOCVD-and MBE-grown materials. The prime motive behind this work is to investigate the suitability of the materials and the laser structure for making TWAs which would use Ti:Sapphire laser at 830 nm as an input source. These optical amplifiers are intended for use in study of quantum fluctuations of devices using semiconductor gain media and implications of these fluctuations on amplifier operation.

GRIN-SCH structures grown by MOCVD and MBE techniques were used to fabricate ridged-waveguide, quasi-index guided laser diodes of stripe widths 10 μm, 8 μm, 6 μm and 4 μm. Room temperature PL measurements were performed with excitation from a HeNe laser source. The MOCVD material exhibited peak emission at 8400 A° with a FWHM of 250 Å. This is in agreement with the specifications provided by the manufacturer. The OSU/ECE MBE material had a peak emission at 8600 Å and a FWHM of 250 Å. An important observation during the PL experiments was that the peak emission was not obtained at the desired wavelength when the 488 nm Ar+ laser was used as the excitation source. But good results were obtained when a HeNe laser source was used. It can be concluded that together with very shallow absorption depth and relatively low

excitation powers for the Ar^+ laser ($\approx$ 4-10 times power of HeNe), fewer carriers reach the quantum well and there is a greater chance of recombination within the barrier regions. Thus at higher temperatures, room temperature for example, the PL signal from the quantum well is likely to become weak due to the sweeping out of the holes by the built in electric field and their conduction away from the highly conductive p-type cladding layer A capacitance voltage technique was used to probe the active region of the MOCVD material for carrier concentration. It was found to be 3E+17 cm^{-3} in the GRIN layer and increased to 1E+18 cm^{-3} in the cladding layer which is again a confirmation of the manufacturer's specification. This technique can thus be effectively used to probe the active regions of shallow anisotropic heterojunctions.

Only pulsed mode operation was performed with square wave pulses of 2.5% duty cycle. I-V characteristics gave a turn-on voltage of about 1.35 V which corresponds closely to the bandgap of the GaAs active region of these devices. The ideality factors of these diodes were found to be only half as compared with that of a commercial diode. L-I analysis of these devices indicated fairly high threshold current values which can be reduced by improving fabrication techniques and optimizing process parameters. The differential quantum efficiency measured for the 10 μm wide MOCVD and MBE lasers were 0.011 W/A and 0.012 W/A, respectively. Differential quantum efficiencies of 0.075 W/A [Ebner] and 0.003 W/A [Eliason] reported previously indicate that these devices are fairly efficient and the materials, in particular the MBE material, looks promising for the fabrication of LDs and TWAs. Spectral gain measurements were calibrated by recording the gain spectrum of a commercial diode lasing at 780 nm. Room temperature lasing was

obtained for the 10 μm, 8 μm and 6 μm wide MOCVD lasers. The 4 μm wide lasers displayed only spontaneous emission. Lasing for the MBE material could be achieved only for the 10 μm wide stripes. Power outputs from the MOCVD lasers were much higher in magnitude than that emitted by the MBE lasers. A maximum of 1.1 mW was recorded from the MOCVD lasers. Due to high threshold currents and fast decay of the devices CW mode operation was not possible. The fast degradation of these devices even under pulsed conditions suggests that effective heat sinking should be provided for the device. Moreover the high percentage of aluminum in the cladding layers could also have led to this condition because aluminum oxidizes rapidly in air and devices mounted on the heat sinks were exposed to air while testing. Better packaging of the devices or operating the existing devices in a nitrogen medium or vacuum can possibly improve the life of the devices. It is also not clear whether the use of spin-on glass as a dielectric instead of CVD SiO_2 or the use of silver epoxy and aluminum wires for bonding instead of gold wire bonds has any direct effect on device performance.

6.2 Future scope

An obvious extension of this work is the fabrication of TWAs using these LDs and to determine internal loss coefficient and gain of structures in fulfillment of the long term goals of this project. AR coatings can be applied to the facets of these LDs and TWA gain saturation characteristics and quantum noise fluctuations can be analyzed. Residual facet reflectivity as low as 0.04% and a saturation output power of +7 dBm at 20 dB signal gain

has been reported for 1.5 μm GaInAsP TWAs [Saitoh et al. 1987]. Previous work done at OSU [Falconer 1995] reports reflectivities in the range of 20.9% to 2.1% for 788 nm commercial laser diodes. Comparable facet reflectivity of the TWAs in the 830 nm range can be attempted and some useful data can be obtained for output power and signal gain. These results can be subsequently used to analyze differences, if any, between the TWAs made in MOCVD and MBE grown materials. This would help in determining the suitability of one material over the other for fabrication of TWAs. Angled facets is certainly a very useful method for reducing facet reflectivity [Zah et al. 1987]. TWAs with stripes angled at 5-7° with the normal can be fabricated on the materials used in this thesis and the above mentioned characterization can be done on such devices. A good comparison can thus be made between TWAs fabricated by different techniques on two different materials. The MBE material certainly has potential for use as good quality laser material. Simpler structures can be grown by MBE for laser fabrication. Standardization of the MBE growth for laser materials would certainly prove cost effective (a 2 inch wafer of MOCVD laser material costs $4000 approximately while a similar laser structure grown in-house by MBE would cost much less) in the long run, particularly for the fabrication of TWAs.

Length dependence of the saturation characteristics in 1.5 μm multi-quantum well TWAs [Eisenstein et al. 1990] has indicated that 1 mm long devices exhibit optimal gain and saturation characteristics. Similar characterization can be performed for different lengths of the 830 nm LDs fabricated here. Fabrication is another area where there is lot of scope for improvement of the quality of devices. As evident from the results in Chapter 4,

the LDs made from MOCVD and the MBE materials had fairly high threshold current densities. This probably stems from the very long devices used for this project. Shorter devices can be made to investigate any appreciable reduction in threshold current. Spin on glass was used as an insulator for device passivation in this thesis. Although this method is fast and simple it may not necessarily be ideal. Alternative methods such as PECVD of SiON can be used instead. Fast degradation of the devices was a major problem especially due to the high percentage of aluminum in the cladding layers of these materials. Effective heat sinking techniques can been explored in order to increase the life of the LDs and TWAs. It would also be interesting to perform measurements of these devices in a nitrogen environment or vacuum and compare results with those reported here. Finally gold wire bonding is an area that can be improved. Aluminum wire bonds were attached to the LDs using a silver epoxy paste. It is undetermined at this stage, whether this could have led to certain deviations in the expected behavior of the devices. In summary future work should include:

- Fabrication of TWAs on both the MBE and MOCVD materials and study of saturation characteristics and quantum noise fluctuations.

- Fabrication of TWAs with reduced facet reflectivities by using methods described in chapter 2, and report the various amplifier characteristics.

- Study of length dependence of saturation characteristics in 830 nm TWAs.

- Use of PECVD of SiON for device passivation.

- Development of effective heat sinking techniques and performing measurements on these devices in N_2 environment or vacuum.

Bibliography

M. J. Adams, J. V. Collins and I. D. Henning, Analysis of semiconductor laser optical amplfiers, *IEE Proceedings*, **132**, Pt. J, 1, 58-63 (1985).

M.G. A Bernard and G. Duraffourg, Phys. Stat. Solidi, **1**, 699 (1969).

P. Bhattacharya, Semiconductor Optoelectronic Devices, (Prentice Hall, NJ, 1994).

H. C. Casey, Jr., M. B. Panish, Heterostructure Lasers part-A: Fundamental Principles, (Academic Press, San Francisco, 1978).

Gregory C. Dente and M. L. Tilton, Modeling broad-area semiconductor optical amplifiers, *IEEE J. Quantum Electron.*, **29**, 1, 76-80 (1993).

P. L. Derry and A. Yariv, Appl. Phys. Lett., **50**, 1773 (1987)

John Ebner, Growth, Fabrication and Modeling of pseudomorphic Laser Diodes, *Doctoral dissertation*, Oregon State University (1989).

Garth W. Eliason, HEMT compatible laser diodes, *Master's thesis*, Oregon State University, (1994).

G. Eisenstein, N. Tessler, U. Koren, J. M. Weisenfeld, G. Raybon and C. A. Burrus, *IEEE Photonics Technol. Lett.*, **2**, 11, 790-791 (1990).

Beate S. Falconer, Grating-tuned external cavity diode lasers, *Master's thesis*, Oregon State University, (1994).

L. Goldberg, D. Mehuys, M. R. Surette and D. C. Hall, High-power, near-diffraction limited large area traveling wave semiconductor amplifiers, *IEEE J. Quantum Electron.*, **29**, 6, 2028-2042 (1993).

Katsuaki Magari, S. kondo, H. Yasaka, Y. Noguchi, T. Kataoka and O. Mikami, A high gain GRIN-SCH optical semiconductor laser amplifier, *IEEE Photonics Technol. Lett.*, **2**, 11, 792-793 (1990).

S. R. Moreno and J. Guitart, Practical method for modelling the nonlinear behaviour of a travelling wave amplifier, *IEE Proceedings J.*, 140, 1, 39-43 (1993).

T. Mukai, T. Saitoh, O. Mikami and T. Kimura, Fabry-Perot cavity type 1.5 μm InGaAsP BH-laser amplifier with small optical mode confinement, *Elecron. Lett.*, **19**, 15, 582-583 (1983).

Robert F. Pierret, Advanced Semiconductor Fundamentals, (Modular Series On Solid State Devices, vol. 6, Addison-Wesley, 1989.

Thomas Plant and M. Raymer, Quantum-noise propagation in long traveling -wave semiconductor amplifiers and superluminescent sources, NSF proposal, (oregon state university).

Clifford R. Pollock, Fundamentals Of Optoelectronics, (Irwin, 1995).

T. Saitoh and T. Mukai, 1.5μm GaInAsP traveling wave semiconductor laser amplifier, *IEEE J. Quantum Electron.*, **QE-23**, 6, 1010-1020 (1987).

T. Saitoh, T. Mukai and Y. Noguchi, Fabrication and gain characteristics of a 1.5 μm InGaAsP traveling-wave amplifier, *First Optoelectronics Conference (OEC '86), PD Tech. Digest*, B 11-2, Tokyo (1986).

T. Saitoh, Y. Suzuki and H. Tanaka, Low noise characteristics of a GaAs-AlGaAs multiple-quantum-well laser amplifier, *IEEE Photonics Technol. Lett.*, **2**, 11, 794-796 (1990).

S. Shimada, H. Ishio, Optical Amplifiers and their Applications, (John Wiley & sons, 1994).

S. Subramanian, B. M. Arora, A. K. Srivastava, G. Fernandes and S. Banerjee, Measurement of band offset of a strained-layer single quantum well by a capacitance-voltage technique, *J. Appl. Phys.*, **74**, 12, 7618-7620 (1993).

Lars Thylen, Amplified spontaneous emission and gain charateristics of Fabry-perot and traveling wave type semiconductor laser amplifiers, *IEEE J. Quantum Electron.*, **24**, 8, (1988).

Jinwei Wang, H. Olesen and K. E. Stubkjaer, Recombination, gain and bandwidth characteristics of 1.3 μm semiconductor laser amplifiers, *IEEE J. Lightwave Tech.*, **LI5**, 1, 184-189 (1987).

Ralph E. Williams, Gallium Arsenide Processing Techniques, (Artech House, 1984).

C. E. Zah, J. S. Osinski, C. Caneau, S. G. Menocal, L. A. Reith, J. Salzman, F. K. Shokoohi and T. P. Lee, Fabrication and performance of 1.5 μm InGaAsP traveling-wave laser amplifiers with angled facets, *Electron. Lett.*, **23**, 19, 990-992 (1987).